



A chemo-mechano-biological modeling framework for cartilage evolving in health, disease, injury, and treatment

Muhammed Masudur Rahman^a, Paul N. Watton^{b,c}, Corey P. Neu^d, David M. Pierce^{a,e,*}

^a Department of Mechanical Engineering, University of Connecticut, Storrs, CT, USA

^b Department of Computer Science & Insigneo Institute for *in silico* Medicine, University of Sheffield, Sheffield, UK

^c Department of Mechanical Engineering and Materials Science, University of Pittsburgh, Pittsburgh, PA, USA

^d Paul M. Rady Department of Mechanical Engineering, University of Colorado, Boulder, CO, USA

^e Department of Biomedical Engineering, University of Connecticut, Storrs, CT, USA

ARTICLE INFO

Article history:

Received 31 October 2022

Revised 8 February 2023

Accepted 10 February 2023

Keywords:

Cartilage

Mechanobiology

Mathematical modeling

Growth and remodeling

Osteoarthritis

Homeostatic adaptation

ABSTRACT

Background and Objective: Osteoarthritis (OA) is a pervasive and debilitating disease, wherein degeneration of cartilage features prominently. Despite extensive research, we do not yet understand the cause or progression of OA. Studies show biochemical, mechanical, and biological factors affect cartilage health. Mechanical loads influence synthesis of biochemical constituents which build and/or break down cartilage, and which in turn affect mechanical loads. OA-associated biochemical profiles activate cellular activity that disrupts homeostasis. To understand the complex interplay among mechanical stimuli, biochemical signaling, and cartilage function requires integrating vast research on experimental mechanics and mechanobiology—a task approachable only with computational models. At present, mechanical models of cartilage generally lack chemo-biological effects, and biochemical models lack coupled mechanics, let alone interactions over time.

Methods: We establish a first-of-its kind virtual cartilage: a modeling framework that considers time-dependent, chemo-mechano-biologically induced turnover of key constituents resulting from biochemical, mechanical, and/or biological activity. We include the “minimally essential” yet complex chemical and mechanobiological mechanisms. Our 3-D framework integrates a constitutive model for the mechanics of cartilage with a novel model of homeostatic adaptation by chondrocytes to pathological mechanical stimuli, and a new application of anisotropic growth (loss) to simulate degradation clinically observed as cartilage thinning.

Results: Using a single set of representative parameters, our simulations of immobilizing and overloading successfully captured loss of cartilage quantified experimentally. Simulations of immobilizing, overloading, and injuring cartilage predicted dose-dependent recovery of cartilage when treated with suramin, a proposed therapeutic for OA. The modeling framework prompted us to add growth factors to the suramin treatment, which predicted even better recovery.

Conclusions: Our flexible framework is a first step toward computational investigations of how cartilage and chondrocytes mechanically and biochemically evolve in degeneration of OA and respond to pharmacological therapies. Our framework will enable future studies to link physical activity and resulting mechanical stimuli to progression of OA and loss of cartilage function, facilitating new fundamental understanding of the complex progression of OA and elucidating new perspectives on causes, treatments, and possible preventions.

© 2023 The Authors. Published by Elsevier B.V.
This is an open access article under the CC BY-NC-ND license
(<http://creativecommons.org/licenses/by-nc-nd/4.0/>)

* Corresponding author.

E-mail address: dmpierce@engr.uconn.edu (D.M. Pierce).

1. Introduction

Osteoarthritis (OA) is a debilitating disease that impacts a significant portion of the population worldwide [1]. OA is the failure of an organ, the synovial joint, wherein the degeneration and loss of cartilage and cartilage function feature prominently. Nearly 20% of people in the US alone suffer from OA [2], which affects quality of life through pain, functional limitations, lost earnings, anxiety, and depression. Treatment remains primarily symptomatic, as no cure yet exists [3]. Despite the impact of the disease itself and an extensive body of research, we do not yet understand the cause or progression of the disease.

Healthy articular cartilage comprises, by percentage wet weight, heterogeneously distributed fluid and electrolytes (68–85%), collagen fibers (15–25%), proteoglycans (PG, 5–10%), and chondrocytes (primary cell type, <4%) [4]. The heterogeneous solid phase of cartilage is the extra-cellular matrix, or ECM, and is made up of a negatively charged proteoglycan mesh and a fiber network of predominantly type II collagen (COL2), both of which contribute to mechanical stiffness of the tissue and permeation of the fluid within the tissue. The remarkable mechanics of healthy cartilage derive from the complex interactions of proteoglycans, collagens, and electrolytic fluid [5,6].

Biomechanical investigations indicate that mechanical stimuli typically experienced in daily activities (i.e. physiological loading) maintain homeostasis in cartilage, while loading schemes outside the physiological range (i.e. non-physiological stimuli) play a key role in the natural history of OA. Both reduced loading (e.g. immobilization) and overloading (e.g. impact trauma) induce molecular, morphological, and mechanical changes that lead to softening, fibrillation, ulceration, and erosion of the cartilage [7]. Under homeostatic physiological loading, chondrocytes maintain a balance between the degradation and synthesis of ECM [8]. Chondrocytes subjected to increased cyclic hydrostatic pressure *in vitro* increase synthesis of proteoglycan; whereas, increased cyclic tension increases their synthesis of collagen [9–13]. Reduced mechanical loading reduces the synthesis activity of the chondrocytes: for example, long-term immobilization leads to ECM loss and cartilage thinning [13]. Excessive mechanical loading also leads to ECM loss [8,13,14]. Both the amplitude and frequency of mechanical loads demonstrate significant effects on the synthesis of ECM molecules and on the biochemical agents that lead to ECM breakdown [9,15].

Chondrocytes not only respond to mechanical loading, but also become “activated” in OA [1], exhibiting increased production of matrix-degrading enzymes, which disrupt the homeostatic balance between synthesis and degradation of ECM constituents [1,7,16]. Pro-inflammatory cytokines, e.g. tumour necrosis factor TNF- α and interleukin IL-1 β , induce chondrocytes to upregulate matrix metalloproteinases (MMPs) and a disintegrin and metalloproteinase with thrombospondin motifs (ADAMTS), causing degradation [7,16,17]. The activity of pro-inflammatory cytokines along with MMPs and ADAMTSs produce more fibronectin fragments (Fn-fs), which in turn provoke further upregulation of pro-inflammatory cytokines [18].

Pro-inflammatory cytokines also directly and indirectly cause apoptosis and necrosis of chondrocytes [19], and chondrocyte apoptosis is a central feature in the degeneration of osteoarthritic cartilage [20]. Chondrocytes in OA cartilage exhibit both proliferative and apoptotic activities [13,20–25], but researchers have shown chondrocyte death correlates with OA across diverse species (e.g. rabbits, dogs, mice, horses, and humans) [20,25–34]. Moreover, the prevalence of apoptotic cells correlates significantly with OA histopathological severity [26,29,31,33,35–38]. The implications of chondrocyte death are significant, given the paucity of chondrocytes even in healthy cartilage tissue.

In OA, remaining viable chondrocytes respond to the upregulation of catabolic agents with attempts to mediate adverse effects by expressing more anabolic cytokines like growth factors, e.g. transforming growth factor (TGF- β) and bone morphogenetic protein (BMP). A large family of growth factors stimulate chondrocytes to synthesize more PG and COL2, and may block the activity of pro-inflammatory cytokines [39]. For example, tissue inhibitors of metalloproteinases (TIMPs) naturally inhibit MMPs and ADAMTS [40,41], and TIMP-3 in particular inhibits both MMPs and ADAMTS in human cartilage [42,43]. The well-established drug suramin [44,45] prevents uptake of TIMP by cells to ensure more TIMP remains present in cartilage. Thus suramin shows great promise to reduce degradation of cartilage and was recently proposed as a treatment for that very reason [46].

Our understanding of OA is far from complete, but research has generated an enormous body of literature on experimental cartilage mechanics and mechanobiology, illuminating pieces of a dynamic whole, and computational models help us understand the bigger-picture puzzle of evolving interplay among mechanical stimuli, biochemical signaling pathways, and cartilage function. Existing computational models put together subsets of the puzzle pieces available in the literature—mechanical, biochemical, functional, and temporal—but none have combined all four. Current computational models of cartilage include mechanical damage [47,48] or degeneration resulting from excessive, repetitive loading [49,50], but do not explicitly include biochemical processes. Mechanobiological models of cartilage that consider the combined effects of mechanical stimuli and chemo-biological actions do not include longitudinal changes in content and organization of constituents or longitudinal changes in volumetric loss [51–54]. Longitudinal changes dictate the condition of cartilage in health, disease, and treatment, and are critical to understanding the big-picture puzzle.

The generalized theory of ‘growth and remodeling’ of soft tissues provides an appealing approach to model tissues in health and disease [55–59], but to date, models using this approach do not encompass the full chemo-mechano-biological complexity of cartilage described in the literature. Previously reported growth-and-remodeling-based models of native and engineered cartilage capture changes in composition and volume, yet do not consider coupled chemical effects [60,61]. Similarly, reported biochemical models of cartilage do not include the full effects of mechanical stimuli [62,63]. Furthermore, to better understand the cause and progression of disease, evidence suggests a need for computational frameworks to also include cell-signaling pathways [64]. We aim to capture the “minimally essential” longitudinally evolving chemo-mechano-biological complexity of cartilage within a computational framework sufficiently flexible to enable future modifications, extensions, and experimental validations.

In this study we establish and exercise a novel 3-D, mathematical framework for modeling the coupled evolution of chemical, mechanical, and biological constituents of cartilage resulting from intra-tissue mechanical and chemical environments, and the health of chondrocytes, and resulting in through-thickness volumetric loss. We couple a new biochemical pathway model, e.g. [65], to our existing constitutive model of cartilage [66,67] to predict the evolution of key cellular and biomolecular species during physiologically relevant mechanical and/or chemical loading. Moreover, we introduce a novel model for homeostasis and adaptation, where cartilage adapts to pathological levels of mechanical stimuli causing perturbations to tissue homeostasis. We exercise our framework both mechanically and chemically to predict the coupled chemo-mechano-biological evolution of key constituents in cartilage and the resulting volumetric loss. First we predict the longitudinal effects of both immobilizing and overloading cartilage, both initiating the progression of OA, and compare our results

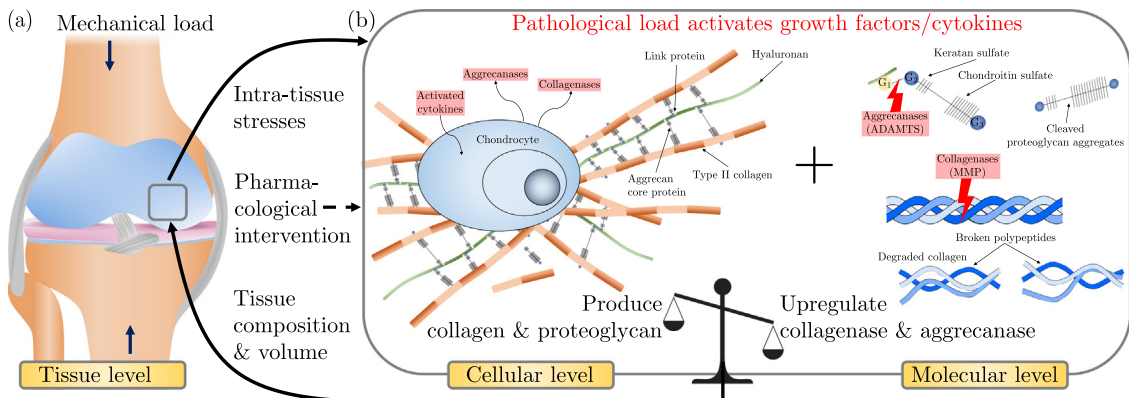


Fig. 1. Coupled tissue-cellular-molecular interactions in our modeling framework for cartilage. (a) Cartilage experiences mechanical loads and chemical treatments during daily activities or pharmacological interventions (see §2.1). (b) Cells (chondrocytes) respond to intra-tissue stresses and chemicals while, at the molecular level, collagenases and aggrecanases cleave polypeptide chains and aggrecan core proteins, respectively (see §2.2). During normal physiological loading, chondrocytes maintain balance between production of structural constituents, i.e. type II collagen and proteoglycan, and their respective degrading proteases, i.e. collagenases and aggrecanases, resulting in tissue homeostasis. Pathological loading causes imbalance with activation of growth factors and pro-inflammatory cytokines and induces chondrocytes to upregulate production of collagenases and aggrecanases, thereby degrading collagen and proteoglycan, thinning cartilage, and altering intra-tissue stresses. Pharmacological interventions, e.g. cell therapy, drug delivery, etc., may alter interactions among tissue, cells, and molecules.

against experimental measurements of thickness. Next, we predict the longitudinal effects of treatments with suramin, an established drug [44,45] recently proposed for treatment of OA, after immobilizing and overloading of cartilage, and after high-impact injury.

2. Methods

Our coupled chemo-mechano-biological framework for modeling the evolution of cartilage is conceptually a 3-D multiscale, i.e. a coupled tissue-cellular-molecular, model comprising a finite-strain, biomechanical model capturing anisotropic growth and remodeling, and a signaling-pathways model capturing the “minimally essential” interactions with chemical and biological constituents, cf. Fig. 1 for a schematic overview.

2.1. Model formulation I: Biomechanical constitutive model of cartilage

2.1.1. Anisotropic description of growth

We exploit the very different time scales between daily activities causing deformations of cartilage, e.g. walking (t in seconds), and progression of OA causing changes in the constituents and subsequently the volume (τ in months or years). With these two time scales we perform a multiplicative decomposition of the total deformation gradient $\mathbf{F}(\tau, t) = \mathbf{F}^e(t)\mathbf{F}^g(\tau)$, cf. Fig. 2.

Chondrocytes within cartilage respond to mechanical and biochemical stimuli and cause growth and degradation of structural and biochemical constituents resulting in volume loss/gain that affects subsequent biomechanical loading conditions. Here the (volumetric) growth deformation gradient $\mathbf{F}^g(\tau)$ captures the volumetric changes ($\det \mathbf{F}^g = \det \mathbf{F} = \hat{v}(\tau)$), where \hat{v} is the normalized volume change. We constrain the elastic deformation gradient $\det \mathbf{F}^e(t) \rightarrow 1$ to ensure incompressible elastic deformations [56].

We introduce through-thickness volume growth (TVG) to model the degradation of cartilage in OA as,

$$\mathbf{F}^g = \mathbf{I} + (\hat{v} - 1)\mathbf{n} \otimes \mathbf{n}, \quad (1)$$

where \mathbf{I} is the identity and \mathbf{n} is a distribution of unit vectors normal to the subchondral bone and attached to the cartilage layer. See Appendix A for further details.

2.1.2. Biomechanical constitutive model of cartilage

To describe the mechanics of cartilage we use a nonlinear, finite-strain constitutive model based on a convex strain energy

function Ψ . We employ a multiplicative split of Ψ into volumetric and isochoric contributions, using the elastic deformation gradient $\mathbf{F}^e = J_S^{(1/3)}\bar{\mathbf{F}}$, where $J_S = \det(\mathbf{F}^e)$ and $\det(\bar{\mathbf{F}}) = 1$, and the elastic right Cauchy-Green tensor $\mathbf{C}^e = J_S^{(2/3)}\bar{\mathbf{C}}$, where $\bar{\mathbf{C}} = \bar{\mathbf{F}}^T\bar{\mathbf{F}}$ [68]. We define the decoupled form,

$$\Psi = U(J_S(t)) + \bar{\Psi}^S, \quad (2)$$

with $U(J_S(t)) = \kappa[J_S(t) - \hat{v}]^2/2$, where κ is a stress-like material parameter used to enforce near incompressibility.

We employ an additive decomposition of the superimposed solid Helmholtz free energy $\bar{\Psi}^S$ into $\bar{\Psi}_{IM}^S$ and $\bar{\Psi}_{FN}^S$, which defines the isotropic matrix and anisotropic fiber network as,

$$\bar{\Psi}^S = (1 - \nu)\hat{\rho}_{pg}\bar{\Psi}_{IM}^S(\bar{I}_1) + \nu\hat{\rho}_{co}\bar{\Psi}_{FN}^S(\bar{I}_4, \mathbf{M}), \quad (3)$$

where $\nu(\tau) = (\nu^0\hat{m}_{co}^f)/[\nu^0\hat{m}_{co} + (1 - \nu^0)\hat{m}_{pg}]$ is the evolving volume fraction of functional collagen with ν^0 its initial volume fraction, $\hat{m}_{pg}(\tau)$ and $\hat{m}_{co}(\tau)$ are the evolving normalized masses of proteoglycan and total collagen, respectively, and $\hat{\rho}_{pg}(\tau)$ and $\hat{\rho}_{co}(\tau)$ are the evolving normalized densities of proteoglycan and collagen, respectively. Additionally, $\hat{m}_{co}(\tau) = \hat{m}_{co}^{fn}(\tau) + \hat{m}_{co}^{dm}(\tau)$, where \hat{m}_{co}^{fn} and \hat{m}_{co}^{dm} are the functional and damaged collagen, respectively.

We define the evolving normalized volume change as,

$$\hat{v} = \nu\hat{\rho}_{co}\hat{m}_{co} + (1 - \nu)\hat{\rho}_{pg}\hat{m}_{pg}, \quad (4)$$

and we assume constant constituent densities, i.e. $\hat{\rho}_{co} = \hat{\rho}_{pg} = 1$ [56]. Since we model volume changes using TVG, \hat{v} equals the normalized change in thickness \hat{h} .

We model the densely packed proteoglycan using a neo-Hookean strain energy function $\bar{\Psi}_{IM}^S(\bar{I}_1) = \mu(\bar{I}_1 - 3)/2$, where μ is Lamé's second parameter, a stress-like material parameter corresponding to the shear modulus of the ground matrix in the reference configuration. We model the anisotropic and nonlinear contributions of networked collagen fibers to the total strain energy of total solid as [66],

$$\bar{\Psi}_{FN}^S(\bar{I}_4, \mathbf{M}) = \int_{\Omega} \rho(\mathbf{M})w(\bar{I}_4)d\Omega, \quad (5)$$

where, $\rho(\mathbf{M})$ is the angular density of fibers (the orientation distribution function) with $1/(4\pi) \int_{\Omega} \rho(\mathbf{M}) d\Omega = 1$ where $\Omega = \mathbf{M} \in \mathbb{R}^3 : |\mathbf{M}| = 1$ is the unit sphere. Without loss of generality we assume $\rho(\mathbf{M})$ produces a isotropic (spherical) distribution in the local orientation of collagen fibers, for more details see Pierce et al.

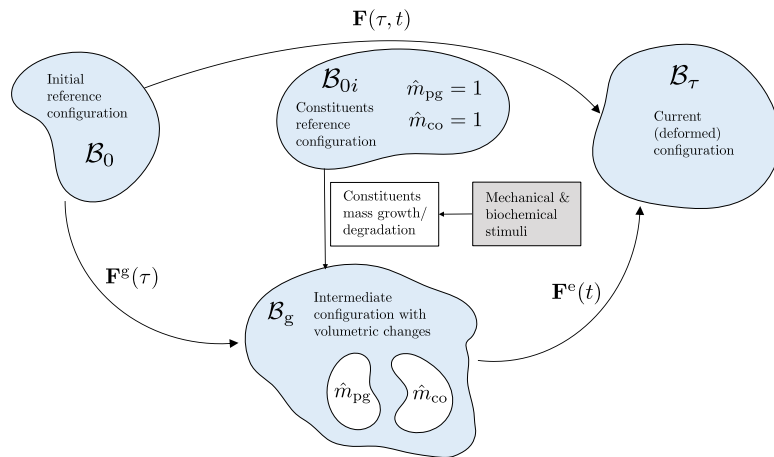


Fig. 2. Kinematics of growth in cartilage. The total deformation gradient $\mathbf{F}(\tau, t)$ maps the reference configuration \mathcal{B}_0 to the current configuration \mathcal{B}_τ . The growth deformation gradient $\mathbf{F}^g(\tau)$ maps the reference configuration \mathcal{B}_0 to the intermediate, stress-free growth configuration \mathcal{B}_g . Mechanical and/or biochemical stimuli cause the growth or degradation of structural components \hat{m}_{pg} and \hat{m}_{co} , representing the normalized proteoglycan (PG) and collagen (CO) content, respectively. The elastic deformation gradient $\mathbf{F}^e(t)$ maps the intermediate, stress-free growth configuration \mathcal{B}_g to the current configuration \mathcal{B}_τ .

Table 1
List of Variables. Symbols and definitions.

Number	Variable	Definition
(a)	\hat{h}	Thickness of cartilage
(b)	\hat{m}_{co}	Mass of collagen including functional and damaged
(c)	\hat{m}_{pg}	Mass of proteoglycan (PG)
(d)	\hat{n}_c	Number of living chondrocytes
(e)	\hat{n}_{nc}	Number of necrotic chondrocytes
(f)	\hat{n}_{hc}	Number of hypertrophic chondrocytes
(g)	\hat{c}_i	Concentration of TIMPs
(h)	\hat{c}_{ca}	Concentration of collagenases (MMPs)
(i)	\hat{c}_{ag}	Concentration of aggrecanases (ADAMTSs)
(j)	\hat{c}_{β}	Concentration of latent growth factors
(k)	\hat{c}_{ip}	Concentration of latent pro-inflammatory cytokines
(l)	\hat{c}_β & \hat{c}_p	Concentration of active growth factors \hat{c}_β (solid line) and active pro-inflammatory cytokines \hat{c}_p (dashed)
(m)	\hat{m}_{co}^{fn}	Mass of functional type II collagen
(n)	\hat{m}_{co}^{dm}	Mass of damaged type II collagen
(o)	\hat{c}_{sm}	Concentration of suramin

[66] and Wang et al. [67]. We define the strain energy of single fibers of reference angular orientation \mathbf{M} as,

$$w(\bar{I}_4) = \frac{k_1}{2k_2} \{ \exp[k_2(\bar{I}_4 - 1)^2] - 1 \} \mathcal{H}(\bar{I}_4 - 1), \quad (6)$$

where the fourth pseudo-invariant \bar{I}_4 is the square of the stretch of a fiber in the direction $\mathbf{m} = \bar{\mathbf{F}}\mathbf{M}$, i.e. $\bar{I}_4(\mathbf{M}) = \lambda^2(\mathbf{M}) = \mathbf{M} \cdot \bar{\mathbf{C}}\mathbf{M}$, $k_1 > 0$ and $k_2 > 0$ are a stress-like material parameter and a dimensionless parameter, respectively, and \mathcal{H} is the Heaviside step function evaluated at $(\bar{I}_4 - 1)$, i.e. the collagen fibers only engage under tensile stretch. We evaluate the integral in (5) numerically [69].

2.2. Model formulation II: Signaling pathways biochemical model

To describe the time evolution of chemical, structural, and cellular species we establish a system of ordinary differential equations (ODEs). We list the chemical, structural, and cellular variables in our model in Table 1, along with a reference number for plotting variables in the results (§3).

We provide a schematic overview of the signaling pathways for our chemo-mechano-biological model in Fig. 3.

Chondrocytes, the primary cell type in cartilage, are quiescent cells, i.e. in healthy equilibrium chondrocytes do not proliferate [70]. Production of chondrocytes (\hat{n}_c) occurs in proportion to the number of chondrocytes and is mediated by the active growth factors \hat{c}_β [71]. Moderate physiological loading maintains cartilage

homeostasis; however, in overloading and reduced loading, a fraction of proliferating cells become hypertrophic and lose their differential phenotype [72,73]. Activated pro-inflammatory cytokines (\hat{c}_p) directly cause cell apoptosis [74]. Therefore, loss of chondrocytes stems from natural decay, phenotypic switching of chondrocytes to hypertrophic chondrocytes (regulated by growth factors), and apoptosis driven by pro-inflammatory cytokines (\hat{c}_p). Consequently, for hypertrophic chondrocytes (\hat{n}_{hc}), production occurs during the phenotypic conversion of normal chondrocytes (\hat{n}_c) to hypertrophic chondrocytes in the presence of active growth factors (\hat{c}_β) which degrade naturally. Additionally, a fraction of living chondrocytes become necrotic during impact loading [75], and go to apoptosis with an exponential decay. We model the time evolution of the normal, hypertrophic, and necrotic chondrocytes in (7)–(9) as

$$\frac{d\hat{n}_c}{d\tau} = (r_1^c + r_2^c \hat{c}_\beta) \hat{n}_c - (r_3^c + r_4^c \hat{c}_\beta + r_5^c \hat{c}_p) \hat{n}_c, \quad (7)$$

$$\frac{d\hat{n}_{hc}}{d\tau} = r_1^{hc} \hat{c}_\beta \hat{n}_c - r_2^{hc} \hat{n}_{hc}, \quad (8)$$

$$\frac{d\hat{n}_{nc}}{d\tau} = -r_1^{nc} \hat{n}_{nc}, \quad (9)$$

where $r_1^c, r_2^c, r_3^c, r_4^c, r_5^c$ are the rate parameters for normal chondrocytes; r_1^{hc}, r_2^{hc} are the rate parameters for hypertrophic chondrocytes; and r_1^{nc} is the rate parameter for necrotic chondrocytes.

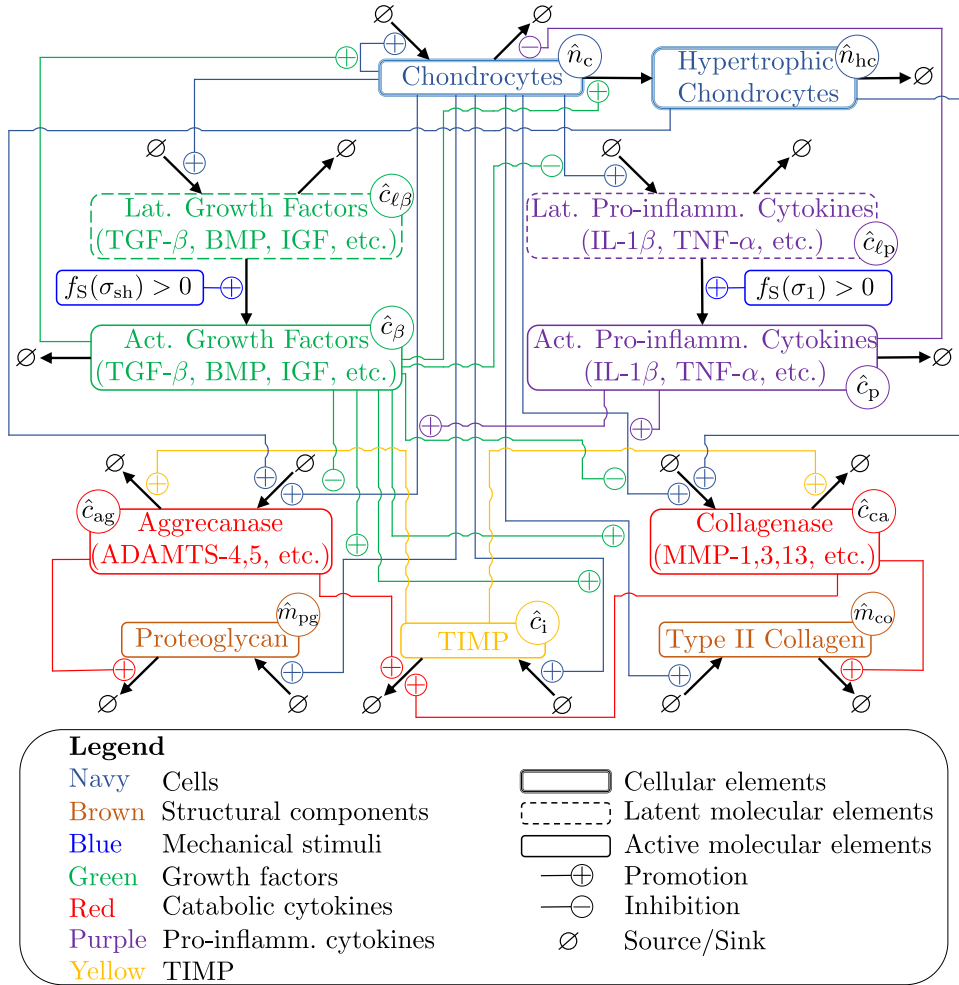


Fig. 3. Schematic of signaling pathways for our chemo-mechano-biological framework. Chondrocytes express structural proteins collagen and proteoglycan, and secret aggrecanase and collagenase to turnover proteoglycan and collagen, respectively. Chondrocytes also produce latent cytokines and growth factors. Non-physiological loading conditions cause activation of latent chemical species. Active pro-inflammatory cytokines upregulate production of both aggrecanase and collagenase including upregulation of latent pro-inflammatory cytokines. Conversely, active growth factors upregulate production of proteoglycan and collagen, proliferate chondrocytes, and promote production of latent growth factors. Tissue inhibitors of matrix metalloproteinases (TIMPs) inhibit production of aggrecanase and collagenase, while active growth factors upregulate production of TIMP.

We introduce two different masses of type II collagen: one is functional, load-bearing collagen \hat{m}_{co}^{fn} and the other is damaged collagen \hat{m}_{co}^{dm} resulting from impact or injury. The latter does not contribute to bearing load. Chondrocytes (\hat{n}_c) express structural proteins, i.e. proteoglycan (\hat{m}_{pg}) and functional collagen (\hat{m}_{co}^{fn}), and active growth factors (\hat{c}_β) upregulate production [39,76]. Proteoglycan and collagen degrade naturally by aggrecanases (\hat{c}_{ag}) and collagenases (\hat{c}_{ca}), respectively. During injuries, functional collagen (\hat{m}_{co}^{fn}) may become damaged (\hat{m}_{co}^{dm}), and this degrades naturally in the presence of collagenases (\hat{c}_{ca}). Total collagen (\hat{m}_{co}) is the sum of \hat{m}_{co}^{fn} and \hat{m}_{co}^{dm} . We model the time evolution of proteoglycan, and functional and damaged collagen in (10)–(12) as

$$\frac{d\hat{m}_{pg}}{d\tau} = (r_1^{pg} + r_2^{pg}\hat{c}_\beta)\hat{n}_c - r_3^{pg}\hat{c}_{ag}\hat{m}_{pg}, \quad (10)$$

$$\frac{d\hat{m}_{co}^{fn}}{d\tau} = (r_1^{co} + r_2^{co}\hat{c}_\beta)\hat{n}_c - r_3^{co}\hat{c}_{ca}\hat{m}_{co}^{fn}, \quad (11)$$

$$\frac{d\hat{m}_{co}^{dm}}{d\tau} = -r_4^{co}\hat{c}_{ca}\hat{m}_{co}^{dm}. \quad (12)$$

In cartilage MMP-1, 3, 13 and ADAMTS-4, 5 are key collagenases and aggrecanases that cause degradation of collagen and proteo-

glycan, respectively [77,78]. Chondrocytes (\hat{n}_c) produce both collagenases (\hat{c}_{ca}) and aggrecanases (\hat{c}_{ag}) and production is upregulated in the presence of active pro-inflammatory cytokines (\hat{c}_p) [79,80]. However, active growth factors (\hat{c}_β) inhibit the production of collagenases and aggrecanases [81]. Hypertrophic cells (\hat{n}_{hc}) express aggrecanases and collagenases [82]. Degradation results from natural decay, decay of the inhibitory complex of TIMP (\hat{c}_i), and both collagenases and aggrecanases. We model the time evolution of collagenases and aggrecanases in (13) and (14), respectively as

$$\frac{d\hat{c}_{ca}}{d\tau} = \left[\frac{r_1^{ca} + r_2^{ca}\hat{c}_p}{1 + r_3^{ca}\hat{c}_\beta} \right] \hat{n}_c + r_4^{ca}\hat{n}_{hc} - (r_5^{ca} + r_6^{ca}\hat{c}_i)\hat{c}_{ca}, \quad (13)$$

$$\frac{d\hat{c}_{ag}}{d\tau} = \left[\frac{r_1^{ag} + r_2^{ag}\hat{c}_p}{1 + r_3^{ag}\hat{c}_\beta} \right] \hat{n}_c + r_4^{ag}\hat{n}_{hc} - (r_5^{ag} + r_6^{ag}\hat{c}_i)\hat{c}_{ag}. \quad (14)$$

Chondrocytes (\hat{n}_c) produce TIMP (\hat{c}_i) and production is upregulated in the presence of active growth factors (\hat{c}_β) [81]. Degradation results from uptake of TIMP by chondrocytes and decay of the inhibitory complex of TIMP with collagenases (\hat{c}_{ca}) and aggrecanases (\hat{c}_{ag}) [83]. Suramin (\hat{c}_{sm}) prevents uptake of TIMP by chondrocytes and ensures more TIMP remains present in cartilage [46], and suramin degrades naturally. We model the time evolution

of TIMP and suramin in (15) and (16), respectively as

$$\frac{d\hat{c}_i}{d\tau} = (r_1^i + r_2^i \hat{c}_\beta) \hat{n}_c - \left[\frac{r_3^i \hat{n}_c}{1 + r_4^i \hat{c}_{sm}} + r_5^i \hat{c}_{ca} + r_6^i \hat{c}_{ag} \right] \hat{c}_i, \quad (15)$$

$$\frac{d\hat{c}_{sm}}{d\tau} = -r_1^{sm} \hat{c}_{sm}. \quad (16)$$

In our model growth factors represent a family of over 30 growth factors, e.g. transforming growth factors or TGF- β 1-3, activins, bone morphogenetic protein (BMP), and growth/differentiation factors (GDFs) expressed in latent forms [81,84,85]. Production of latent growth factors ($\hat{c}_{\ell\beta}$) occurs in proportion to the current number of normal chondrocytes (\hat{n}_c) and production is upregulated in the presence of active growth factors (\hat{c}_β). Growth factors are bound by latency-associated peptides (LAPs) and latent TGF- β binding proteins (LTBPs). These bonds need to be broken to activate growth factors [81]. Active growth factors are minimally present in unloaded cartilage; however, mechanical forces such as shear or compressive loading activate latent growth factors [73,85-87]. Degradation of latent growth factors therefore occurs during the conversion of latent growth factors to the active form, caused by pathological mechanical stimuli ($f_S(\sigma_{sh}) > 0$, see §2.3) and by natural decay. Consequently, the production of active growth factors \hat{c}_β occurs during this process. Active growth factors also decay exponentially. We model the time evolution of latent and active growth factors in (17) and (18), respectively as

$$\frac{d\hat{c}_{\ell\beta}}{d\tau} = (r_1^{\ell\beta} + r_2^{\ell\beta} \hat{c}_\beta) \hat{n}_c - (r_3^{\ell\beta} + r_4^{\ell\beta} f_S(\sigma_{sh})) \hat{c}_{\ell\beta}, \quad (17)$$

$$\frac{d\hat{c}_\beta}{d\tau} = r_1^\beta f_S(\sigma_{sh}) \hat{c}_{\ell\beta} - r_2^\beta \hat{c}_\beta. \quad (18)$$

Two key cytokines involved in joint inflammation are IL-1 β and TNF- α , and these are expressed in latent form [88]. Active cytokines upregulate production of latent pro-inflammatory cytokines [79,80]. Normal chondrocytes (\hat{n}_c) produce latent pro-inflammatory cytokines ($\hat{c}_{\ell p}$), and these are upregulated by active pro-inflammatory cytokines (\hat{c}_p). However, active growth factors (\hat{c}_β) inhibit production of latent pro-inflammatory cytokines [81]. Necrotic cells (\hat{n}_{nc}) also upregulate production of latent pro-inflammatory cytokines. Degradation results from natural decay and conversion of latent pro-inflammatory cytokines to the active form (caused by pathological mechanical stimuli). Physiolog-

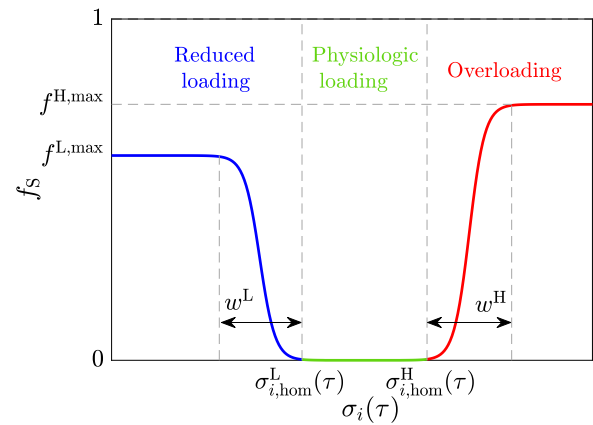


Fig. 4. Schematic of mechanical stimulus function f_S . The stimulus function $f_S \in [0, 1]$ is a double sigmoidal function of the mechanical stimulus $\sigma_i(\tau)$ ($i \in \{sh, 1\}$) and the high and low homeostatic thresholds, $\sigma_{i,hom}^H(\tau)$ and $\sigma_{i,hom}^L(\tau)$, respectively. In normal physiological loadings, $f_S = 0$ while in pathological loadings $f_S > 0$ and leads to activation of growth factors and cytokines in the biochemical signaling pathway model (see §2.2).

(20), respectively as

$$\frac{d\hat{c}_{\ell p}}{d\tau} = \left[\frac{r_1^{\ell p} + r_2^{\ell p} \hat{c}_p}{1 + r_3^{\ell p} \hat{c}_\beta} \right] (1 + r_4^{\ell p} \hat{n}_{nc}) \hat{n}_c - [r_5^{\ell p} + r_6^{\ell p} f_S(\sigma_1)] \hat{c}_{\ell p}, \quad (19)$$

$$\frac{d\hat{c}_p}{d\tau} = r_1^p f_S(\sigma_1) \hat{c}_{\ell p} - r_2^p \hat{c}_p. \quad (20)$$

2.3. Model formulation III: Homeostasis and adaptation to mechanical stimuli

Under physiological loading conditions, chondrocytes maintain homeostatic balance and the constituents of cartilage remain unchanged. However, during non-physiological loading, homeostatic balance is lost. Injurious or pathological mechanical stimuli, e.g. excessive shear or tensile stresses, cause activation of both growth factors and pro-inflammatory cytokines [79]. In our model, we consider pathological levels of first principal stress (σ_1) and maximum shear stress (σ_{sh}) as two mechanical stimuli that causes activation of latent pro-inflammatory cytokines and growth factors, respectively. To incorporate mechanical stimuli into our signaling pathways biochemical model (see §2.2), we introduce a piecewise continuous, well-shaped mechanical stimulus function, f_S , defined as

$$f_S = \begin{cases} f^{L,max}, & \text{if } \sigma_i(\tau) \leq \sigma_{i,hom}^L(\tau) - w^L \\ f^L(\sigma_i(\tau), \sigma_{i,hom}^L(\tau), w^L), & \text{if } \sigma_{i,hom}^L(\tau) - w^L < \sigma_i(\tau) < \sigma_{i,hom}^L(\tau) \\ 0, & \text{if } \sigma_{i,hom}^L(\tau) \leq \sigma_i(\tau) \leq \sigma_{i,hom}^H(\tau) \\ f^H(\sigma_i(\tau), \sigma_{i,hom}^H(\tau), w^H), & \text{if } \sigma_{i,hom}^H(\tau) < \sigma_i(\tau) < \sigma_{i,hom}^H(\tau) + w^H \\ f^{H,max}, & \text{if } \sigma_i(\tau) \geq \sigma_{i,hom}^H(\tau) + w^H \end{cases}, \quad (21)$$

ical tensile loading inhibits the nuclear factor kappa B (NF- κ B) signaling, which activates pro-inflammatory cytokines [89,90]. Hence, we hypothesize that $f_S(\sigma_1) = 0$ during physiological loading, and non-physiological (both immobilization and overloading) loading activates latent pro-inflammatory cytokines ($f_S(\sigma_1) > 0$, see §2.3). Production of active pro-inflammatory cytokines \hat{c}_p occurs during conversion of latent pro-inflammatory cytokines ($\hat{c}_{\ell p}$) caused by pathological mechanical stimuli, i.e. $f_S(\sigma_1) > 0$. Active pro-inflammatory cytokines degrade naturally. We model the time evolution of latent and active pro-inflammatory cytokines in (19) and

where f^L and f^H are sigmoidal functions, $\sigma_i(\tau)$ is the mechanical stimulus at evolution time τ with $i \in \{sh, 1\}$, $\sigma_{i,hom}^L(\tau)$ and $\sigma_{i,hom}^H(\tau)$ represent low (L) and high (H) homeostatic thresholds of mechanical stimulus $\sigma_i(\tau)$ (subscript comma does not indicate differentiation). The constants $f^{L,max} \in (0, 1]$ and $f^{H,max} \in (0, 1]$ are maximum values of f_S under low and high pathological loading, and w^L and w^H are parameters controlling the width of the sigmoidal transition zones from physiological to pathological loading. During normal, physiological loading conditions, $f_S = 0$. We provide a schematic representation of the mechanical stimulus function at a fixed time τ in Fig. 4.

We assume that the homeostatic thresholds may adapt [91] and we implement this using an averaging scheme taking into account the temporal history of stimuli [92]. For immobilizing, we adapt the low homeostatic threshold $\sigma_{i,\text{hom}}^L(\tau)$ while $\sigma_i(\tau) \leq \sigma_{i,\text{hom}}^L(\tau)$ as follows,

$$\sigma_{i,\text{hom}}^L(\tau) = \begin{cases} \sigma_{i,\text{hom}}^{L,0}, & \text{if } \tau \leq \tau_{\text{del}}^L, \\ \min \left[\sigma_{i,\text{hom}}^{L,0}, \left(\int_{\tau-\tau^L}^{\tau} \sigma_i(\tau) d\tau / \tau^L \right) \right], & \text{if } \tau > \tau_{\text{del}}^L \end{cases} \quad (22)$$

where $\sigma_{i,\text{hom}}^{L,0}$ denotes the prescribed initial values of the lower homeostatic threshold. The parameters τ_{del}^L and τ^L control the time delay and temporal averaging period for adaptation to immobilizing, respectively. Similarly, for overloading we adapt the high homeostatic threshold $\sigma_{i,\text{hom}}^H(\tau)$ while $\sigma_i(\tau) \geq \sigma_{i,\text{hom}}^H(\tau)$ as follows,

$$\sigma_{i,\text{hom}}^H(\tau) = \begin{cases} \sigma_{i,\text{hom}}^{H,0}, & \text{if } \tau \leq \tau_{\text{del}}^H, \\ \max \left[\sigma_{i,\text{hom}}^{H,0}, \left(\int_{\tau-\tau^H}^{\tau} \sigma_i(\tau) d\tau / \tau^H \right) \right], & \text{if } \tau > \tau_{\text{del}}^H \end{cases} \quad (23)$$

where $\sigma_{i,\text{hom}}^{H,0}$ denotes the prescribed initial value of the high homeostatic threshold. The parameters τ_{del}^H and τ^H control the time delay and temporal averaging period for adaptation to overloading, respectively. See [Appendix B](#) for further details

2.4. Computational implementation

We exploited the very different time scales between daily activities, e.g. walking (seconds), and progression of OA (months to years), which allows iterative rather than simultaneous solutions. To exercise the coupled model we solved the system of equations ensuring quasi-static mechanical equilibrium of a unit cube (in the absence of body forces), i.e. $\text{div } \boldsymbol{\sigma} = \mathbf{0}$, undergoing compression representative of loads acting within the human knee joint during walking, immobilizing, overloading, and injury. We solved this system of equations iteratively using an explicit method. We translated compressive forces acting within the human knee joint to an equivalent force F acting on the unit cube (1 mm^3) as [93],

$$F = M \left(\frac{a_s}{a_k} \right) m_b g \quad (24)$$

where M is an activity-specific load multiplier, $a_s = 1 \text{ mm}^2$ is the contact area of the unit cube, $a_k = 958 \text{ mm}^2$ is the average contact area within a human knee, $m_b = 70.8 \text{ kg}$ is the average human body mass [94], and $g = 9.81 \text{ m/s}^2$ is the gravitational constant. The load multipliers M for normal walking and downhill walking are 3.9 and 8, respectively [95]. We define the normal homeostatic loading range as $4 \leq M \leq 8$ for a healthy adults. Consequently, we computed the initial values of the low and high homeostatic thresholds, $\sigma_{i,\text{hom}}^{L,0}$ and $\sigma_{i,\text{hom}}^{H,0}$, using $M = 4$ and $M = 8$, respectively. For illustrative examples, we consider immobilizing (reduced loading) as $M = 0.5$ and overloading as $M = 10$.

Given the current state of mechanical equilibrium we solved the system of ODEs (7)–(16) for the current time τ using a backward (finite difference) Euler approach. The initial condition for the normalized quantities \hat{n}_c , \hat{m}_{co} , \hat{m}_{pg} , \hat{c}_{ca} , \hat{c}_{ag} , \hat{c}_i , $\hat{c}_{\ell\beta}$, and $\hat{c}_{\ell\alpha}$ was unity. Hypertrophic and necrotic chondrocytes are generally not present in healthy cartilage and so \hat{n}_{hc} and \hat{n}_{nc} started at zero. The active chemical species \hat{c}_p and \hat{c}_β also started at zero since they are not activated unless cartilage is injured. Finally, the concentration of suramin \hat{c}_{sm} was set to zero except when prescribed explicitly. Each simulation starts from negative time, i.e. month -1 , representing the healthy homeostatic condition prior to pathological loadings which start from month zero.

We implemented both mechanical equilibrium and the coupled chemo-mechano-biological model using MATLAB R2021b (The

Table 2
Material Parameters. Values and units [96].

Parameter	Value	Unit
μ	1	MPa
k_1	3	MPa
k_2	8	—
v^0	0.8	—

Mathworks, Natick, MA). We solved for mechanical equilibrium (at time t) at each cartilage state (at time τ) using `fsolve` within MATLAB. After preliminary testing to ensure convergence, we chose the time step τ as 0.01 months.

2.5. Model parameters

2.5.1. Biomechanical constitutive model of cartilage

We provide the material parameters for the constitutive model of cartilage (§2.1.2) in [Table 2](#) [96].

2.5.2. Signaling pathways biochemical model

Each of the constituents outlined in §2.2 and [Table 1](#) naturally decay. We estimate the corresponding rate parameter for the decay of the i^{th} constituent λ^i as,

$$\lambda^i = \frac{\ln 2}{t_{1/2}^i}, \quad (25)$$

where $t_{1/2}^i$ is the half-life of the i^{th} constituent.

In healthy cartilage chondrocytes undergo apoptosis at the rate of approximately 0.15% per day, which results the half life of approximately 15 months [97]. We estimate the rate parameter r_3^c using (25). In homeostasis the rate of production of chondrocytes equals the rate of death, and therefore, we set $r_1^c = r_3^c$. A portion of proliferating chondrocytes become hypertrophic, therefore the degradation rate parameter r_4^c should equal the rate parameter for production of hypertrophic chondrocytes, i.e. $r_4^c = r_1^{hc}$.

The half-lives of type II collagen and proteoglycan are approximately 90 years and 25 years, respectively [98–100]. We estimate r_3^{co} and r_3^{pg} using (25). We set the rate parameters for production $r_1^{co} = r_3^{co}$ and $r_1^{pg} = r_3^{pg}$ since the type II collagen and proteoglycan content remains constant in homeostasis.

Anabolic and catabolic cytokines show a range of half-lives ranging from approximately 0.08 to 15 h [101–106]. We estimate the half-life of the latent and activated cytokines as 10 h and estimate $r_3^{\ell\beta}$ and r_2^{β} using (25). To balance the production and degradation in homeostasis we set $r_1^{\ell\beta} = r_3^{\ell\beta}$. We also set $r_4^{\ell\beta} = r_1^{\beta}$ to account for activation of growth factors from the latent form. Similarly, we estimate $r_5^{p\beta}$ and r_2^p for latent and active pro-inflammatory cytokines, respectively, using (25). To balance the production and degradation in homeostasis we set $r_1^{p\beta} = r_5^{p\beta}$. We also set $r_6^{p\beta} = r_1^p$ to account for activation of cytokines from the latent form.

The half-life of MMPs is approximately 120 h [63], from which we estimate r_5^{sm} using (25). The half-lives of both of ADAMTSs and TIMPs are approximately 3.6 h [107,108], from which we estimate r_5^{ag} and r_3^i using (25). TIMP, collagenase, and aggrecanase form a complex [63] which has degradation rate parameters r_6^{ca} and r_6^{ag} . To balance the production and degradation in homeostasis we set $r_1^{\text{ca}} = r_5^{\text{ca}} + r_6^{\text{ca}}$ and $r_1^{\text{ag}} = r_5^{\text{ag}} + r_6^{\text{ag}}$. The half-life of suramin is approximately 14.5 days [45], from which we estimate r_1^{sm} using (25).

We set the remaining-rate parameters (r_2^c , r_5^c , r_1^{co} , r_2^{pg} , $r_2^{\ell\beta}$, $r_2^{p\beta}$, $r_3^{\ell\beta}$, $r_4^{\ell\beta}$, r_2^{ca} , r_3^{ca} , r_4^{ca} , r_2^{ag} , r_3^{ag} , r_4^{ag} , and r_2^i) by using numerical experiments simulating immobilizing and overloading conditions detailed in §3.1 and by prescribing how rates of production are upregulated or downregulated relative to homeostatic levels. To sim-

Table 3

Cellular and structural rate parameters. Definitions, values, and references.

Parameter	Definition	Value [month ⁻¹]	Notes and References
r_1^c	Rate of baseline chondrocytes proliferation	4.5×10^{-2}	Equal r_3^c ; balancing source/sink terms at homeostasis
r_2^c	Rate of chondrocytes population dynamics sensitivity to anabolic cytokines and growth factors	4×10^{-1}	Combined anabolic cytokines and growth factor effects [81,112]
r_3^c	Rate of baseline chondrocytes death	4.5×10^{-2}	Extrapolating the apoptosis rate of normal chondrocytes [97]
r_4^c	Rate of proliferating chondrocytes converting into hypertrophic chondrocytes	1×10^{-2}	Growth factors cause proliferation; fraction of the proliferating chondrocytes become hypertrophic [81,113]
r_5^c	Rate of activated pro-inflammatory cytokines driven cell death	1×10^{-1}	Pro-inflammatory cytokines cause cell death [74]
r_1^{hc}	Rate of proliferating chondrocytes converting into hypertrophic chondrocytes	1×10^{-2}	Equal to r_4^c ; cellular species conversion; Growth factors cause proliferation; fraction of the proliferating chondrocytes become hypertrophic
r_2^{hc}	Rate of baseline hypertrophic chondrocytes death	4.5×10^{-1}	Fraction of normal chondrocytes become necrotic due to high impact injurious loading
r_1^{nc}	Rate of baseline necrotic chondrocytes death	1	Equal r_3^c ; balancing source/sink terms at homeostasis
r_1^{co}	Rate of baseline collagen deposition by chondrocytes	6.4×10^{-4}	Growth factors increase collagen deposition [114]
r_2^{co}	Rate of growth factors driven increase in collagen deposition by chondrocytes	1×10^{-1}	Based on the half lives of collagen in cartilage [98]
r_3^{co}	Rate of collagenase-driven functional collagen degradation	6.4×10^{-4}	Damaged collagen degrades faster than functional collagen
r_4^{co}	Rate of collagenase-driven damaged collagen degradation	1	Equal r_2^{co} ; balancing source/sink terms at homoeostasis
r_1^{pg}	Rate of baseline proteoglycan deposition by chondrocytes	2.3×10^{-3}	Growth factors increase PG deposition [114]
r_2^{pg}	Rate of growth factors driven increase in proteoglycan deposition by chondrocytes	1×10^{-1}	Based on the half lives of PG in cartilage [99,100]
r_3^{pg}	Rate of aggrecanase-driven proteoglycan degradation	2.3×10^{-3}	

plify model parameterization, we suppose growth factors cause negligible inhibitory effects and set $r_3^{ca} = r_3^{ag} = r_3^{cp} = 1$. Similarly, we suppose growth factors cause negligible upregulation of TIMPs and set $r_1^i \approx 10^{-3} r_1^p$.

We assume hypertrophic chondrocytes express more collagenases than aggrecanases [109]. Thus we set $r_4^{ca} = 10r_1^{ca}$ and $r_4^{ag} = r_1^{ag}$ for illustration. We set the upregulation of latent pro-inflammatory cytokines as five times the basal level when half of cells become necrotic, this requires $r_2^{cp} = 5$. We assume growth factors can increase the proliferation of chondrocytes, and thus for illustration $r_2^c = 0.4$ to yield a 20% increase. We also assume active pro-inflammatory cytokines accelerate cell death, and doubling the rate requires $r_5^c = 0.1$.

We adjusted the model parameters so that there is a modest upregulation (approximately a factor of 2) of latent growth factors due to the presence of active growth factors, and so that active growth factors remain a small proportion of latent form (approximately 1–2%). Similarly, a small fraction of latent cytokines become active.

The rate parameters r_2^{co} and r_2^{pg} relate to the upregulation of collagen and proteoglycan production in the presence of active growth factors, respectively. The parameters r_2^{ca} and r_2^{ag} relate to the upregulation of collagenase and aggrecanase in the presence of active cytokines. Given the long half-lives of collagen and proteoglycan, we required collagenase/aggrecanase levels to increase significantly (30–120×) in pathological conditions to match the rate of tissue loss observed in experimentally. In addition, we assumed that tissue loss maintains the relative proportions of collagen and proteoglycan during degradation. We assume that in the presence of growth factors, production of collagen and proteoglycan can increase by several fold; for illustration collagen production increases by a factor of four and proteoglycan production by a factor of two for typical peak levels of growth factors during pathological loading. We performed parameter studies on these parameters to fit the experimental data on cartilage thickness from baseline to 24 months during immobilizing (Vanwanseele et al. [110]) and during overloading (Frobell [111]).

Tables 3 and 4 list the complete rate parameters of our signaling pathways biochemical model.

2.5.3. Homeostasis and adaptation to mechanical stimuli

With load multipliers bounding the homeostatic range, i.e. $M = 4$ and $M = 8$, we calculate the corresponding maximum shear stresses and the first principal stresses and use these values to prescribe initial homeostatic thresholds $\sigma_{sh,hom}^{L,0} = 1.0$ MPa, $\sigma_{sh,hom}^{H,0} = 1.9$ MPa, $\sigma_{1,hom}^{L,0} = 0.67$ MPa, and $\sigma_{1,hom}^{H,0} = 1.3$ MPa. Both immobilizing (Vanwanseele et al. [110]) and overloading (Frobell [111]) lead to cartilage loss that stabilizes *in vivo*. When the change in thickness of cartilage stabilizes we assume it is in homeostasis, and this assumption allows us to estimate parameters in (22) and (23) controlling the evolution of the homeostatic thresholds. Based on experimental observations of cartilage adapting to pathological loading, cartilage does not adapt instantaneously and achieves a new homeostasis on the order of months [118], and thus the time delay parameters must be on the order of days to weeks. For illustration we assume $\tau_{del}^L = \tau_{del}^H = 0.5$ months and numerically determine the temporal averaging periods τ^L and τ^H to fit experimental data [110,111]. See Appendix C for further details. Additionally, we set $f^{L,max} = 0.60$ and $f^{H,max} = 0.63$ to reflect the initial rates of change in thickness during immobilizing and overloading, respectively.

2.6. Numerical simulations

To exercise our coupled chemo-mechano-biological model of evolving osteoarthritis in cartilage we complete three numerical studies. We designed these studies to calibrate and test the minimally essential functions of our coupled model. In all studies we simulated chemo-mechano-biological evolution of cartilage for 24 months, except for our third study (with application of suramin alone in varying concentrations) because cartilage reached equilibrium within 12 months.

Study 1: Cartilage response to immobilizing and overloading.

We perform two simulations to fit experimental data on longitudinal thickness of cartilage from the *in-vivo* studies by Vanwanseele et al. [110] and Frobell [111] for immobilizing and overloading, respectively. To simulate immobilizing and overloading conditions we set the load multiplier to $M = 0.5$ and $M = 10$, cf. (24), respec-

Table 4**Biochemical rate parameters.** Definitions, values, and references.

Parameter	Definition	Value [month ⁻¹]	Notes and References
$r_1^{\ell\beta}$	Rate of baseline latent growth factors secretion by chondrocytes	5.0×10^1	Equal $r_3^{\ell\beta}$; balancing source/sink
$r_2^{\ell\beta}$	Rate of latent growth factor secretion by chondrocytes mediated by active growth factors	5.0×10^3	
$r_3^{\ell\beta}$	Rate of baseline degradation of latent growth factors	5.0×10^1	Based on half lives of growth factors in cartilage [102–104]
$r_4^{\ell\beta}$	Rate of latent growth factor converting to active form by mechanical stimuli	5.0×10^{-1}	Active growth factor has very low concentration in cartilage [115]
r_1^{β}	Rate of latent growth factor converting to active form by mechanical stimuli	5×10^{-1}	Equal to $r_4^{\ell\beta}$, cellular species conversion
r_2^{β}	Rate of baseline degradation of active growth factor	5.0×10^1	Equal $r_3^{\ell\beta}$; same rate of degradation as latent growth factors
$r_1^{\ell p}$	Rate of baseline latent pro-inflammatory cytokines secretion by chondrocytes	5.0×10^1	Equal $r_5^{\ell p}$; balancing source/sink
$r_2^{\ell p}$	Rate of latent pro-inflammatory cytokines secretion by chondrocytes triggered by active cytokines	5.0×10^3	
$r_3^{\ell p}$	Rate of latent pro-inflammatory cytokines inhibition by active growth factors	1	
$r_4^{\ell p}$	Rate of baseline latent pro-inflammatory cytokines secretion by necrotic chondrocytes	5	
$r_5^{\ell p}$	Rate of baseline degradation of latent pro-inflammatory cytokines	5.0×10^1	Based on half lives of pro-inflammatory cytokines in cartilage [101,105,106]
$r_6^{\ell p}$	Rate of latent pro-inflammatory cytokines converting to active form by mechanical stimuli	1	Active pro-inflammatory cytokines has very low concentration in cartilage
r_1^p	Rate of latent pro-inflammatory cytokines converting to active form by mechanical stimuli	5×10^{-1}	Equal to $r_6^{\ell p}$, cellular species conversion
r_2^p	Rate of baseline degradation of active pro-inflammatory cytokines	5.0×10^1	Equal $r_5^{\ell p}$; same rate of degradation as latent pro-inflammatory cytokines
r_1^{ca}	Rate of baseline collagenase secretion by chondrocytes	4.6	Equal $r_5^{ca} + r_6^{ca}$; balancing source/sink terms at homeostasis
r_2^{ca}	Rate of pro-inflammatory cytokines-driven upregulation in collagenase secretion by chondrocytes	6.0×10^2	
r_3^{ca}	Rate of growth factors-driven downregulation in collagenase secretion by chondrocytes	1	
r_4^{ca}	Rate of baseline collagenase secretion by hypertrophic chondrocytes	1.0×10^2	Hypertrophic chondrocytes express collagenases [116]
r_5^{ca}	Rate of baseline collagenase degradation	4.2	Based on the half lives of collagenase in cartilage [63,117]
r_6^{ca}	Rate of TIMP-mediated collagenase degradation	$0.1r_4^{ca} = 4.2 \times 10^{-1}$	Assuming additional 10% degradation by TIMP complex of collagenase and aggrecanase [63]
r_1^{ag}	Rate of baseline aggrecanase secretion by chondrocytes	1.4×10^2	Equal $r_5^{ag} + r_6^{ag}$; balancing source/sink terms at homeostasis
r_2^{ag}	Rate of pro-inflammatory cytokines-driven upregulation in aggrecanase secretion by chondrocytes	5.0×10^3	
r_3^{ag}	Rate of growth factors-driven downregulation in aggrecanase secretion by chondrocytes	1	
r_4^{ag}	Rate of baseline aggrecanase secretion by hypertrophic chondrocytes	1.0×10^2	Hypertrophic chondrocytes express aggrecanases [116]
r_5^{ag}	Rate of baseline aggrecanase degradation	1.4×10^2	Based on the half lives of aggrecanase in cartilage [107]
r_6^{ag}	Rate of TIMP-mediated aggrecanase degradation	4.2×10^{-1}	Equal to r_6^{ca} ; additional degradation by TIMP complex of collagenase and aggrecanase [63]
r_1^i	Rate of baseline TIMP secretion by chondrocytes	1.4×10^2	
r_2^i	Rate of growth factors-driven increase in TIMP by chondrocytes	1×10^{-1}	Equal $r_1^i + r_4^i + r_5^i$; balancing source/sink
r_3^i	Rate of baseline TIMP degradation and uptake by chondrocytes	1.4×10^2	Based on the half lives of aggrecanase in cartilage [108]
r_4^i	Rate of suramin driven downregulation of TIMP degradation	1.0×10^2	Suramin inhibits the uptake of TIMP by chondrocytes [46]
r_5^i	Rate of TIMP degradation of TIMP and collagenase complex	4.2×10^{-1}	Equal r_6^{ca}
r_6^i	Rate of TIMP degradation of TIMP and aggrecanase complex	4.2×10^{-1}	Equal r_6^{ag}
r_1^{sm}	Rate of baseline suramin degradation	1.4	Based on the half lives of suramin in blood stream [45]

tively. Before immobilizing and overloading conditions ($\tau < 0$), we set the load multiplier $M = 6$ to define physiological loading.

Study 2: Treatment with suramin during immobilizing and overloading. We perform longitudinal simulations of immobilizing ($M = 0.5$) and overloading ($M = 10$) and include three different treatments (concentrations) of suramin, specifically $\hat{c}_{sm} = 0.1$, $\hat{c}_{sm} = 0.5$, and $\hat{c}_{sm} = 1$. We compare the results without treatment of suramin to the dose-dependent responses with suramin.

Study 3: Treatments with suramin after injury. We perform simulations of healthy cartilage experiencing high-impact injurious loading at $\tau = 0$ months. Prior to injury, we simulate normal healthy conditions with the load multiplier $M = 6$, cf. (24). Cartilage then loses 26% of the living chondrocytes and of the functional type II collagen due to the injury [75]. Post injury, we immobilize cartilage for $\tau = 6$ months ($M = 0.5$) and thereafter go back to normal healthy conditions ($M = 6$). With this mechanical his-

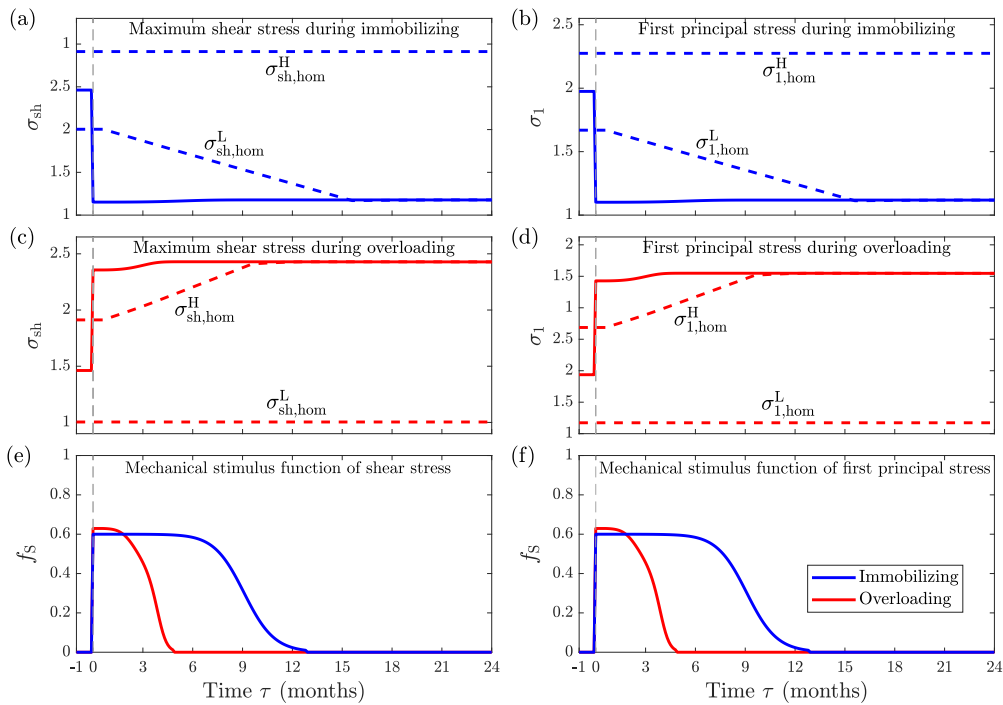


Fig. 5. Evolution of intra-tissue mechanics while cartilage evolves in immobilizing and overloading, represented by blue and red curves respectively. Specifically: (a) maximum shear stress σ_{sh} during immobilizing, (b) first principal stress σ_1 during immobilizing, (c) maximum shear stress σ_{sh} during overloading, (d) first principal stress σ_1 during overloading, (e) mechanical stimulus functions of shear stress f_S , and (f) mechanical stimulus functions of first principal stress f_S . (For interpretation of the references to colour in this figure legend, the reader is referred to the web version of this article.)

tory we perform three sub-studies by varying treatments based on suramin. In sub-study 1 we apply three different concentrations of suramin to cartilage, specifically $\hat{c}_{sm} = 0.1$, $\hat{c}_{sm} = 0.5$ and $\hat{c}_{sm} = 1$, during immobilizing (i.e. six months total). We compare the results without suramin treatment to the dose-dependent responses with suramin. In sub-study 2 we apply the highest concentration of suramin ($\hat{c}_{sm} = 1$) for three different application times including and beyond immobilizing, specifically 12, 18, and 24 months. We compare the results of suramin treatment only during immobilizing to the dose-dependent responses including and beyond immobilizing. In sub-study 3 we apply the highest concentration of suramin ($\hat{c}_{sm} = 1$) for the longest application time (24 months) accompanied by three different externally applied concentrations of active growth factors, specifically $\hat{c}_\beta = 0.01$, $\hat{c}_\beta = 0.02$, $\hat{c}_\beta = 0.03$. We compare the results without active-growth-factor treatment to the dose-dependent responses with externally applied active growth factors.

3. Results

3.1. Study 1: Cartilage response to immobilizing and overloading

In this study we simulate progressive thinning and stabilization of cartilage in response to both immobilizing and overloading. In both simulations we use identical rate parameters with the exception of the parameters which control the rates of adaptation of the homeostatic thresholds ($\tau^L = 15$ versus $\tau^H = 9$ months). In what follows we describe in mechanistic detail how our multi-scale, chemo-mechano-biological model accounts for the progressive thinning and stabilization of cartilage. In Fig. 5 we illustrate the evolution of intra-tissue mechanical variables, homeostatic thresholds, and stimulus functions that drive pathological remodeling. In Fig. 6 we illustrate the evolution of cartilage thick-

ness, and cellular and molecular species. See Table 1 for a description of the cellular and molecular variables.

In immobilizing conditions ($\tau > 0$), due to the load multiplier $M = 0.5$ (see §2.4), the maximum shear stress ($\sigma_{sh} = 0.15$ MPa) and first principal stress ($\sigma_1 = 0.10$ MPa) fall below minimum homeostatic thresholds $\sigma_{sh,hom}^{L,0} = 1.0$ MPa and $\sigma_{1,hom}^{L,0} = 0.67$ MPa. This activates the stimulus functions, i.e. $f_S(\sigma_{sh}, \sigma_{sh,hom}^L) > 0$ and $f_S(\sigma_1, \sigma_{1,hom}^L) > 0$, and drives pathological remodeling pathways leading to cartilage thinning. However, we gradually adapt the homeostatic thresholds $\sigma_{sh,hom}^L$ and $\sigma_{1,hom}^L$ towards those of the (current) perturbed mechanical environment (see §2.3) (Fig. 5(a) and (b)). Consequently, the values of the mechanical stimulus functions f_S gradually reduce towards zero over time (Fig. 5(e) and (f)), cf. Appendix B. This novel feature of our framework facilitates remodeling of cartilage towards a new homeostasis. We adjusted the time parameter controlling the rate of adaptation of the homeostatic threshold so that the final cartilage thickness matches experimental data [110], for immobilizing this requires $\tau^L = 15$ months. If $\tau^L < 15$, the thickness of cartilage stabilizes more quickly and the final reduction in thickness is reduced, cf. Appendix C.

In immobilizing conditions, chemo-mechano-biological pathways drive the reduction in tissue thickness. Pathological levels of intra-tissue mechanical stimuli Fig. 5(e) and (f)) activate latent growth factors and latent pro-inflammatory cytokines (Fig. 6(l)); the increased concentrations of these molecular species feed back to upregulate their latent forms (17) and (19) respectively (Figs. 6(j) and (k)). The increase in growth factors upregulates TIMP production and promotes chondrocyte proliferation (7), and a fraction of proliferating cells become hypertrophic (8) (Fig. 6(f)). The active pro-inflammatory cytokines cause cell death leading to a reduction in normal, living chondrocytes by 28% over nine months (Fig. 6(d)). In addition, cytokines upregulate collagenases and aggrecanases (Fig. 6(h) and (i)) which drives

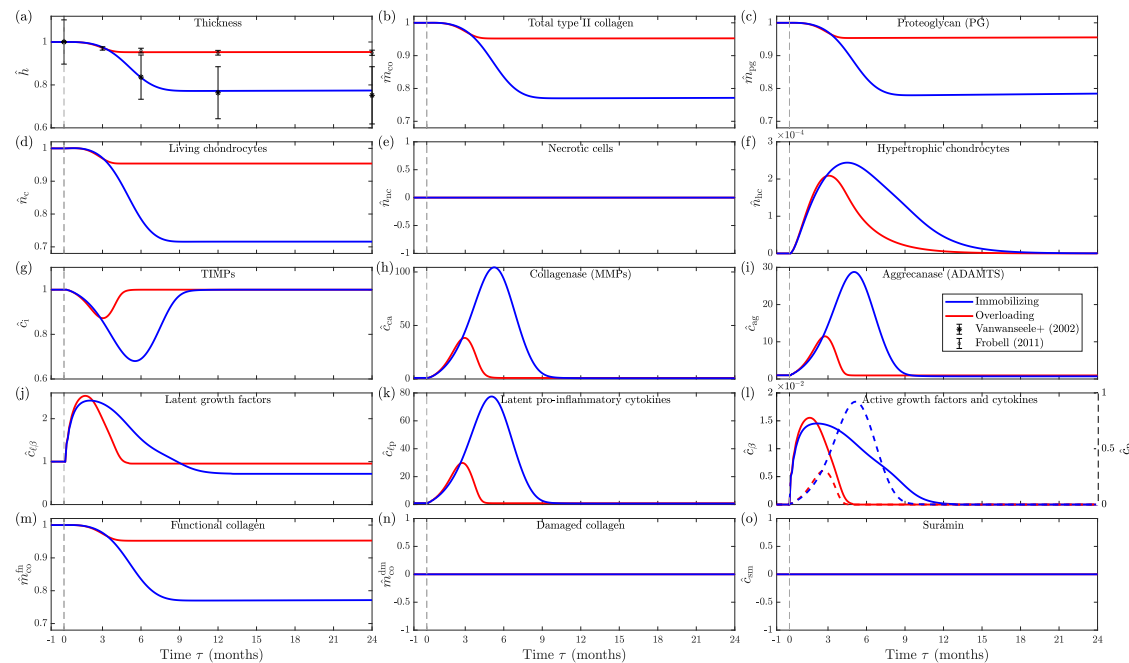


Fig. 6. Cartilage evolves in immobilizing and overloading represented by blue and red blue curves respectively. Time $\tau < 0$ months represents healthy homeostatic conditions. Immobilizing and overloading starts at $\tau = 0$ months and continues for $\tau = 24$ months, causing activation of pro-inflammatory cytokines (19) and growth factors (17). Activated cytokines promote increased production of latent cytokines which eventually convert to active forms. The increase in activated cytokines causes upregulation of collagenases and aggrecanases, which results in degradation of collagen and proteoglycan, respectively. As a result the overall thickness of cartilage changes during immobilizing and overloading, and the result provides a good fit to experimental data from Vanwanseele et al. [110] and Frobell [111], respectively. See Table 1 for a description of the variables. (For interpretation of the references to colour in this figure legend, the reader is referred to the web version of this article.)

degradation of collagen and proteoglycan (Fig. 6(b) and (c)). The concentrations of collagenases and aggrecanases peak after five months ($\hat{c}_{ca} \approx 110$ and $\hat{c}_{ag} \approx 31$). After nine months, collagen and proteoglycan stabilize following a loss of approximately 24% and 21% of their initial content and consequently there is a similar decrease in the thickness of cartilage, cf. (4) (Fig. 6(a)).

In overloading conditions ($\tau > 0$), due to the load multiplier $M = 10$ (see §2.4), the mechanical environment exceeds the homeostatic thresholds and the mechanical stimulus functions $f_s(\sigma_{sh}, \sigma_{sh,hom}^H)$ and $f_s(\sigma_1, \sigma_{1,hom}^H)$ drive pathological remodeling. These functions have initial values of 0.63 and decay to zero (5(e) and (f)) as homeostatic thresholds $\sigma_{sh,hom}^H$ and $\sigma_{1,hom}^H$ adapt (Fig. 5(c) and (d)). The action of the pathway model follows similar to that in immobilizing. However, we adjusted the time parameter controlling the rate of adaptation of the (high) homeostatic threshold so that the final cartilage thickness matches experimental data [111], and this requires that the adaptation occurs more quickly, i.e. $\tau^H = 9$ months. In response to overloading, pathologically elevated intra-tissue mechanical stimuli activate the latent growth factors and latent pro-inflammatory cytokines (Fig. 6(l)) leading to chondrocyte death and hypertrophy, upregulation of collagenases and aggrecanases, and degradation of collagen and proteoglycan. As the values of the stimuli functions f_s drop to near zero due to adaptation of the homeostatic thresholds, the activated chemical species also drop and the thickness of cartilage stabilizes. Note that while the total load acting on cartilage remains fixed, the maximum shear stress and first principal stress increase slightly to 2.35 and 1.57 MPa, respectively, due to the evolving volume and composition (Fig. 5(c) and (d)).

3.2. Study 2: Treatment with suramin during immobilizing and overloading

In this study we examine the impact of the drug suramin on the remodeling response of cartilage while subject to immobilizing

and overloading using the calibration from §3.1. In Figs. 7 and 8 we illustrate the evolution of cellular and molecular species in immobilizing and overloading conditions, respectively, over 24 months and with various doses (concentrations) of suramin where the blue curve represents no treatment with suramin, and the red, green, and magenta curves represent treatments with suramin in concentrations of $\hat{c}_{sm} = 0.1, 0.5$, and 1, respectively.

During immobilizing conditions, our framework predicts that higher concentrations of suramin produce greater improvements in the retention of cartilage thickness Fig. 7(a)). Specifically comparing no treatment to treatment with the highest concentration of suramin ($\hat{c}_{sm} = 1$), we see a reduction in the loss of cartilage thickness of approximately 25%. In our framework the action of suramin (Fig. 7(o)) inhibits uptake of TIMP by chondrocytes (see (15) and consequently it leads to increases in TIMP within cartilage (Fig. 7(g)). The concentration of TIMP reaches peak values after approximately one month and subsequently decreases due to the increase of collagenase and aggrecanase (Fig. 7(h) and (i), respectively), which follow the levels of active cytokines (Fig. 7(l)). The presence of elevated TIMP downregulates the peak concentrations of collagenases and aggrecanases by up to 15% and 1.2%, respectively. As collagenase and aggrecanase subsequently reduce towards basal levels between six and nine months, TIMP starts to increase again (Fig. 7(g)) due to the continued application of suramin. To summarize, application of suramin leads to increases in TIMP, decreases in collagenases and aggrecanases, less degradation of collagen and proteoglycan (Fig. 7(b) and (c), respectively), and thus less cartilage loss. During overloading conditions, with no suramin treatment, cartilage thickness decreases by approximately 5%. However, with the application of suramin, our framework predicts cartilage thickness can recover (Fig. 8(a)). Mechanistically, the framework works in a similar way to that in immobilizing. During overloading, the constant application of suramin (Fig. 8(o)) inhibits uptake of TIMP by chondrocytes (15) which subsequently increases TIMP (Fig. 8(g)). With the highest concentra-

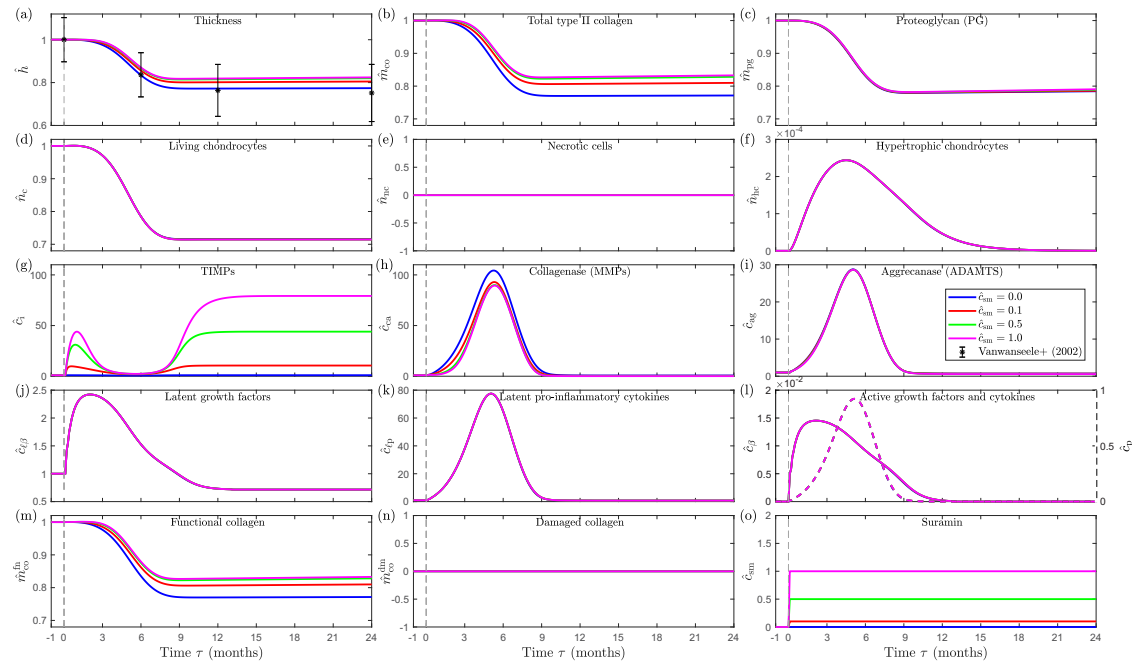


Fig. 7. Cartilage evolving in immobilizing conditions with and without treatments of suramin - suramin produces dose-dependent reductions in loss of cartilage. The blue curve represents no treatment with suramin. The red, green, and magenta curves represent treatments with suramin in concentrations of $\hat{c}_{\text{sm}} = 0.1, 0.5$, and 1 , respectively. Time $\tau < 0$ months represents healthy, homeostatic conditions. Immobilizing starts at $\tau = 0$ months and continues for $\tau = 24$ months while we hold the concentration of suramin constant. Suramin inhibits degradation of TIMP which downregulates collagenases and aggrecanases such that less collagen and proteoglycan degrades. Overall this results in less degradation of cartilage and subsequently improvements in thickness of cartilage versus without treatment, cf. Vanwanseele et al. [110]. See Table 1 for a description of the variables. (For interpretation of the references to colour in this figure legend, the reader is referred to the web version of this article.)

tion of suramin, i.e. $\hat{c}_{\text{sm}} = 1$, TIMP reaches a peak value after one month, but decreases thereafter due to increases of collagenases and aggrecanases (Fig. 8(h) and (i), respectively). The presence of elevated TIMP downregulates the peaks of collagenases and aggrecanases by approximately 50% and 4%, respectively. As \hat{c}_{ca} and \hat{c}_{ag} reduce to basal levels at approximately five months TIMP starts to increase (Fig. 8(g)). Due to the increase of TIMP and the decreases in collagenases and aggrecanases, we see less degradation of collagen and proteoglycan (Fig. 8(b) and (c), respectively), and thus less cartilage loss.

3.3. Study 3: Treatment with suramin after injury

In this study we examine the impact of three different suramin-based treatments on the remodeling response of cartilage while subject to injury, immobilizing, and return to normal walking using the calibration from §3.1. In Fig. 9 we illustrate the evolution of intra-tissue mechanical variables, homeostatic thresholds, and mechanical stimulus functions that drive pathological remodeling. Immobilizing following impact injury significantly alters the intra-tissue mechanics of cartilage. The stress magnitudes reduce below the homeostatic thresholds (Fig. 9(a) and (b)), and hence the values of the mechanical stimulus functions, $f_S(\sigma_{\text{sh}})$ and $f_S(\sigma_1)$, increase (Fig. 9(c) and (d), respectively). These increases drive activation of latent pro-inflammatory cytokines and growth factors, and subsequent tissue remodeling. After six months of immobilizing, the patient goes back to normal walking, thus restoring intra-tissue stresses to homeostatic levels and reducing the mechanical stimulus functions to zero. However, note that cartilage now experiences higher intra-tissue stresses σ_{sh} and σ_1 versus the initial state due to injury-driven changes in the constituents and total volume.

In Fig. 10 (sub-study 1) we illustrate the evolution of cellular and molecular species over 12 months with various doses (concentrations) of suramin where the blue curve represents no treat-

ment, and the red, green, and magenta curves represent treatments with suramin in concentrations of $\hat{c}_{\text{sm}} = 0.1, 0.5$, and 1 , respectively. The high-impact injury at $\tau = 0$ damages 26% of the functional collagen (Fig. 10(n)) and causes an equal quantity of chondrocytes to become necrotic (see Fig. 10(e)), and damaged collagen and necrotic cells subsequently degrade following (7) and (12). The sudden loss of chondrocytes causes the latent growth factors to initially drop (Fig. 10(j)). However, the ensuing activation of latent pro-inflammatory cytokines and growth factors (Fig. 10(l)) feeds back to upregulate their latent forms. The presence of necrotic cells also contributes to upregulation of latent pro-inflammatory cytokines (19). After immobilizing, latent forms of growth factors and cytokines return to baseline levels. Suramin acts to inhibit uptake of TIMP by chondrocytes and thus increased concentrations of suramin elevate TIMP (Fig. 10(g)). Increased TIMP in turn reduces the peak in collagenase (Fig. 10(h)) and thus reduces loss of collagen (Fig. 10(m)). The first peak in TIMP occurs at approximately one month and then it drops to a local minimum as collagenases and aggrecanases reach a maximum. As levels of collagenases and aggrecanases decrease, TIMP again increases due to application of suramin. We stop the application of suramin after six months and levels of TIMP subsequently fall to zero. Overall, we see an approximately 4% reduction in the loss of volume (Fig. 10(a)) comparing outcomes at 12 months without treatment and with treatment at the highest concentration of suramin ($\hat{c}_{\text{sm}} = 1$).

In Fig. 11 (sub-study 2) we illustrate the evolution of cellular and molecular species over 24 months with the highest previous concentration of suramin $\hat{c}_{\text{sm}} = 1$, and with various time periods for application of the treatment where the blue, red, green, and magenta curves represent applications for 6, 12, 18, and 24 months total. Prolonging the time period for application of suramin (Fig. 11(o)) prolongs the elevation of TIMPs (Fig. 11(g)). This in turn leads to downregulation of collagenases (Fig. 11(h)) and aggrecanase (Fig. 11(i)) relative to baseline levels. However, the net effect yields only marginal increases in collagen (Fig. 11(b)) and

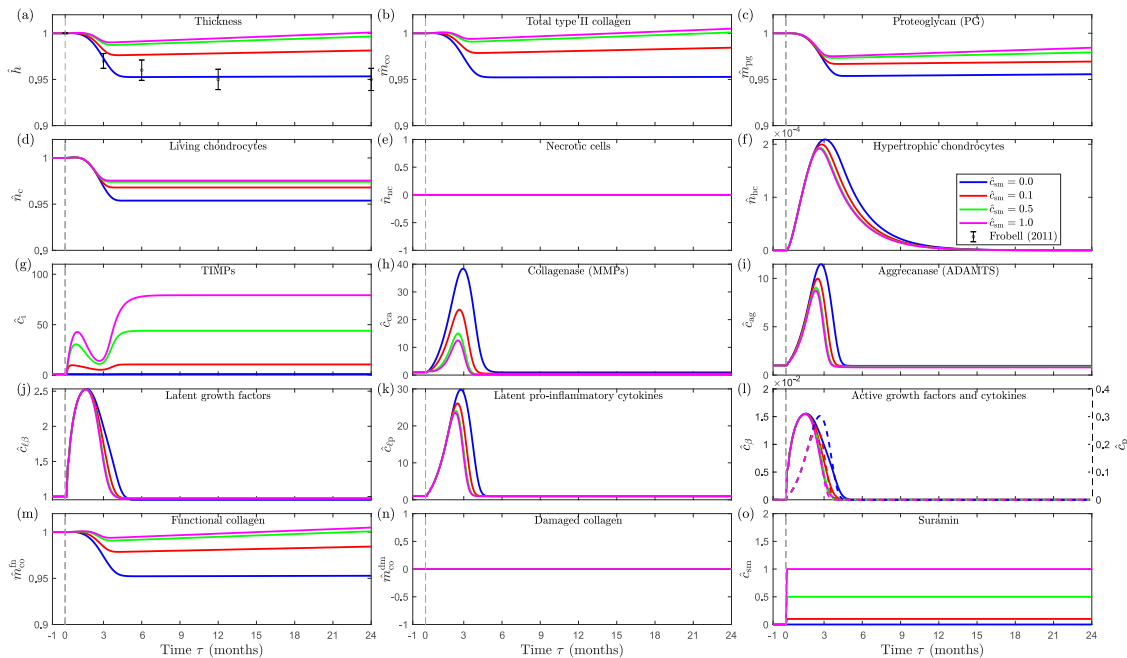


Fig. 8. Cartilage evolving in overloading conditions with and without treatments of suramin - suramin produces dose-dependent reductions in loss of cartilage. The blue curve represents no treatment with suramin. The red, green, and magenta curves represent treatments with suramin in concentrations of $\hat{c}_{\text{sm}} = 0.1, 1$, and 10 , respectively. Time $\tau < 0$ months represents healthy, homeostatic conditions. Overloading starts at $\tau = 0$ months and continues for $\tau = 24$ months while we hold the concentration of suramin constant. Suramin inhibits degradation of TIMP which downregulates collagenases and aggrecanases such that less collagen and proteoglycan degrades. Overall this results in less degradation of cartilage and subsequently improvements in thickness of cartilage versus without treatment, cf. Frobell [111]. See Table 1 for a description of the variables. (For interpretation of the references to colour in this figure legend, the reader is referred to the web version of this article.)

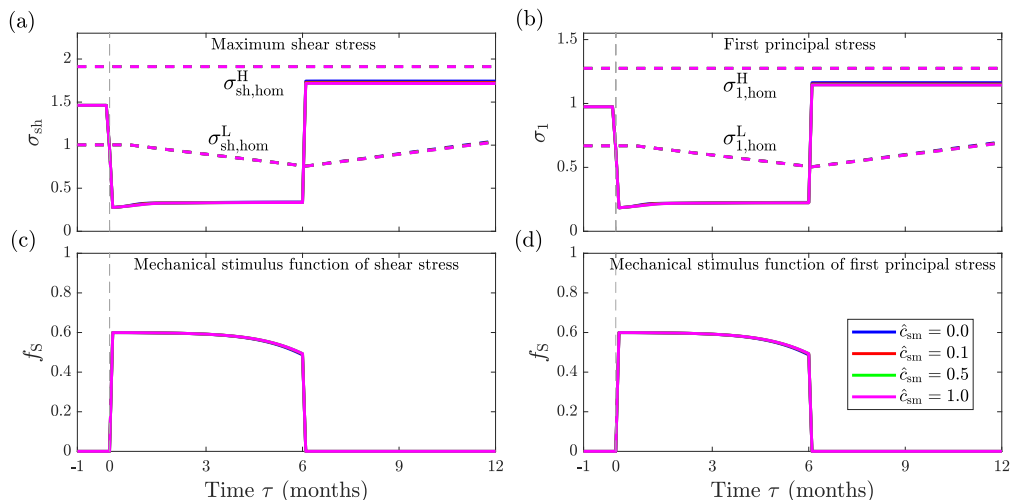


Fig. 9. Evolution of intra-tissue mechanical variables while cartilage evolves after injury and during recovery, with and without treatments of suramin. Cartilage experiences a high-impact injury at $\tau = 0$ months, followed by immobilization for $\tau = 6$ months after which the patient goes back to normal walking. During immobilizing the injured cartilage receives treatments of suramin. Specifically: (a) maximum shear stress σ_{sh} , (b) first principal Stress σ_1 , (c) mechanical stimulus functions of shear stress f_s , and (d) mechanical stimulus functions of first principal stress f_s .

proteoglycan (Fig. 11(c)), and thus only marginal improvements in final tissue thickness (Fig. 11(a)) due to the low production rates of collagens and proteoglycans in non-pathological conditions. Notably, the activation of both growth factors and pro-inflammatory cytokines is unaffected by the time period of application (Fig. 11(l)).

Finally, in Fig. 11 (sub-study 3) we illustrate the evolution of cellular and molecular species over 24 months with the highest previous concentration of suramin $\hat{c}_{\text{sm}} = 1$ and with various doses (concentrations) of active growth factors where the blue curve represents no treatment with active growth factors, and the red, green, and magenta curves represent treatments with externally applied active growth factors in concentrations of $\hat{c}_{\beta}^{\text{ext}} =$

0.01, 0.02, and 0.03, respectively. In all simulations the application of specified treatments remains constant for 24 months. Increases in the concentration of externally applied active growth factors (Fig. 12(l)) increases in latent growth factors (Fig. 12(j)), promotes cell proliferation (Fig. 12(d)), and upregulates production of collagen and proteoglycan (Fig. 12(b) and (c)). Moreover, the presence of latent/active growth factors down regulates latent/active pro-inflammatory cytokines (Fig. 12(k) and (l)) and consequently down regulates collagenase and aggrecanase (Fig. 12(h) and (i)). Overall both collagen and proteoglycan increase (Fig. 12(b) and (c)) resulting in recovery of cartilage thickness (Fig. 12(a)). In this injury and recovery scenario after 24 months, treatment with suramin and externally applied active growth factors ($\hat{c}_{\beta}^{\text{const}} = 0.03$) results in a fi-

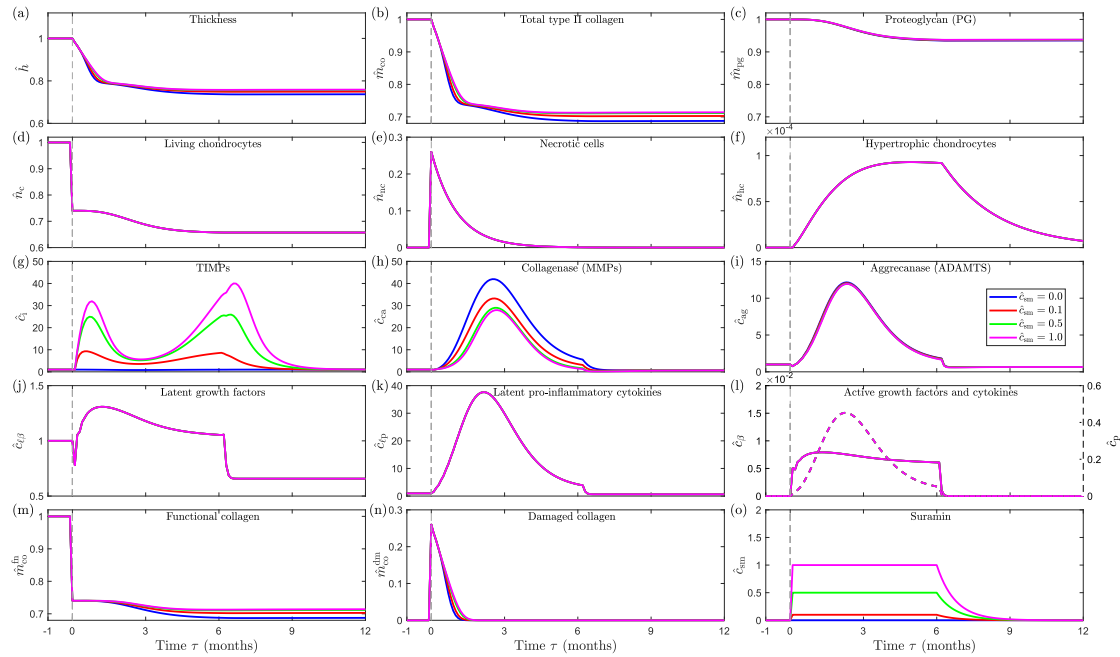


Fig. 10. Cartilage evolving in injury and recovery with various concentrations of suramin. The blue curve represents no treatment with suramin. The red, green, and magenta curves represent treatments of suramin in concentrations of $\hat{c}_{sm} = 0.1, 0.5$, and 1 , respectively. Time $\tau < 0$ months represents healthy homeostatic conditions. High-impact injury occurs at $\tau = 0$ months, thereafter cartilage is immobilized for six months (while we hold the concentration of suramin constant) and then returns to normal walking conditions for an additional six months (without suramin). Suramin inhibits degradation of TIMP which downregulates collagenases and aggrecanases such that less collagen and proteoglycan degrades. Overall this results in less degradation of cartilage and subsequently improvements in thickness of cartilage versus without treatment. See Table 1 for a description of the variables. (For interpretation of the references to colour in this figure legend, the reader is referred to the web version of this article.)

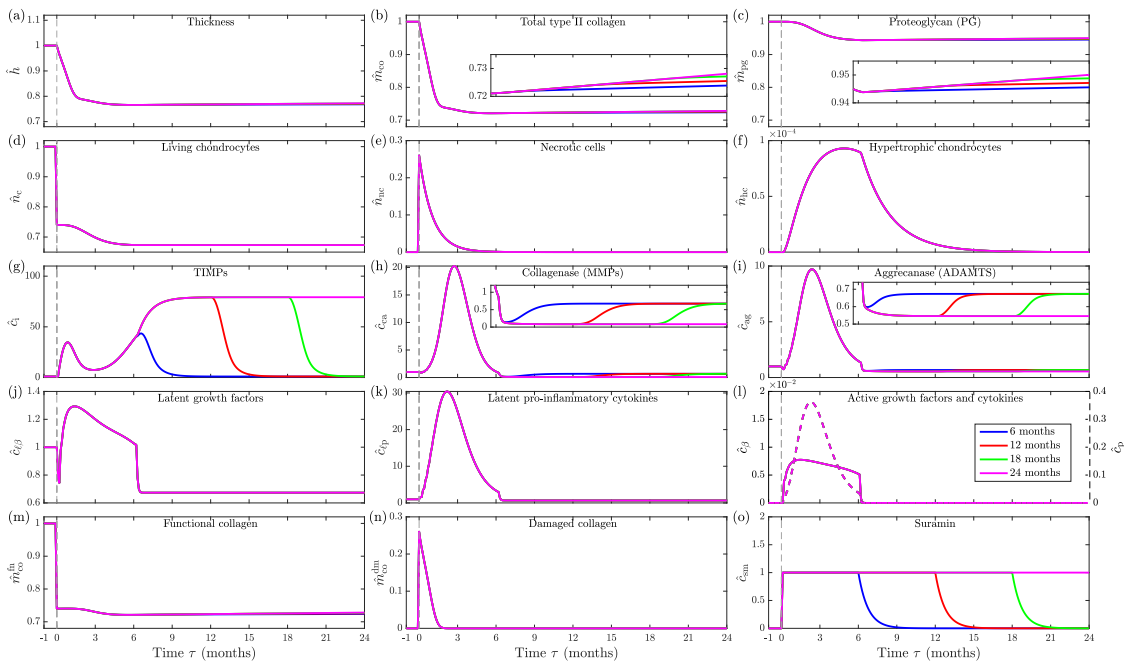


Fig. 11. Cartilage evolving in injury and recovery with various time periods for application of suramin at concentration $\hat{c}_{sm} = 1$. The blue, red, green, and magenta curves represent treatments of suramin in concentration $\hat{c}_{sm} = 1$ for time periods for 6, 12, 18, and 24 months total, respectively. Time $\tau < 0$ months represents healthy homeostatic conditions. High-impact injury occurs at $\tau = 0$ months, thereafter cartilage is immobilized for six months and then returns to normal walking conditions for an additional 18 months (while we hold the concentration of suramin constant throughout). Suramin inhibits degradation of TIMP which downregulates collagenases and aggrecanases such that marginally less collagen and proteoglycan degrades. Overall this results in marginally less degradation of cartilage and subsequently marginal improvements in thickness of cartilage versus without treatment. Subfigures (b), (c), (h), and (i) include inset images expanding the y-axis for clarity. See Table 1 for a description of the variables. (For interpretation of the references to colour in this figure legend, the reader is referred to the web version of this article.)

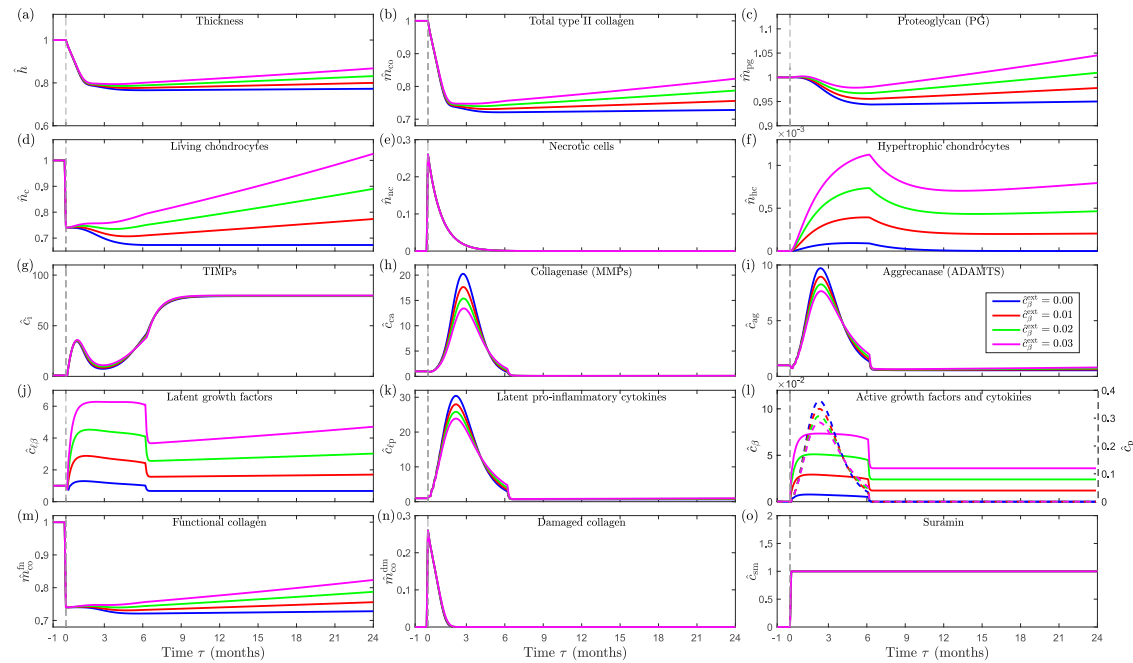


Fig. 12. Cartilage evolving in injury and recovery with application of suramin at concentration $\hat{c}_{sm} = 1$ combined with various concentrations of active growth factors. The blue curve represents treatment with suramin but no externally applied active growth factors. The red, green, and magenta curves represent treatment with suramin combined with treatments of externally applied active growth factors in concentrations of $\hat{c}_p^{ext} = 0.01, 0.02$, and 0.03 , respectively. Time $\tau < 0$ months represents healthy homeostatic conditions. High-impact injury occurs at $\tau = 0$ months, thereafter cartilage is immobilized for six months and then returns to normal walking conditions for an additional 18 months (while we hold the concentration of suramin and the concentration of externally applied active growth factors constant throughout). Suramin inhibits degradation of TIMP which downregulates collagenases and aggrecanases such that less collagen and proteoglycan degrades. Increases in the total active growth factors increases the latent growth factors which in turn promotes cell proliferation and further up regulates production of collagens and proteoglycans. Moreover, the presence of latent/active growth factors down regulates latent/active pro-inflammatory cytokines and consequently down regulates collagenase and aggrecanase, thus increasing collagens and proteoglycans. Overall this results in less degradation of cartilage and subsequently improvements in thickness of cartilage versus without treatment of externally applied active growth factors. See Table 1 for a description of the variables. (For interpretation of the references to colour in this figure legend, the reader is referred to the web version of this article.)

nal thickness of cartilage at 87% of the original thickness versus 77% without externally applied active growth factors (Fig. 12(a)).

4. Discussion

Our work establishes a first-of-its kind virtual cartilage: a new modeling framework that considers time-dependent, chemo-mechano-biologically induced turnover of key constituents resulting from biochemical, mechanical, and/or biological activity. Our novel computational framework is the first to fully integrate a non-linear, large-strain constitutive model for the mechanics of cartilage with a model of the cell-signaling pathways which drive growth-and-remodeling of cartilage, and which in turn alter the mechanical response. In formulating our model of the cell signaling pathways we included the “minimally essential” yet complex chemical and mechanobiological mechanisms within cartilage to predict the evolution of key constituents. To achieve this, we established and incorporated into the framework a novel model of homeostatic adaptation of cells to pathological mechanical stimuli. We also pioneered a new application for kinematics of anisotropic growth to simulate the through-thickness degradation clinically observed as cartilage thinning—loss quantified in the model as negative growth. With representative rate parameters, our simulations of immobilizing and overloading cartilage successfully predict the loss of cartilage volume (presented as thickness) quantified in previously reported experimental studies, e.g. Vanwanseele et al. [110] and Frobell [111]. To demonstrate use of the framework to simulate clinical treatments, we modeled the use of suramin, recently proposed as a potential treatment for OA due to its inhibition of uptake of TIMPs by chondrocytes [46], for treatment of osteoarthritic or otherwise degenerated cartilage. We simulated immobilizing, overloading, and injuring cartilage, and showed treat-

ments of suramin result in dose-dependent reductions in thinning of cartilage. A notable simulation result suggested suramin would be less effective for cartilage subjected to impact injury (relative to overloading or immobilization) and motivated us to explore different treatment combinations. As a result, we showed that for cartilage subjected to impact injury, treatments of suramin combined with active growth factors facilitate faster and greater recovery of cartilage after thinning, an outcome we would not have pursued without the simulation results made possible by our new framework.

4.1. Studies 1–3: Numerical simulations of cartilage evolving in health, disease, injury, and treatment

In Study 1 (§3.1), consistent with available experimental data, our simulations showed that during pathological loading cartilage establishes a new homeostasis that includes a thinned but stable cartilage volume. Motivated by the (sparse) experimental data available in the literature, we hypothesized that chondrocytes can adapt to pathological mechanical stimuli. Our model thus assumes the homeostatic threshold values shift in response to pathological mechanical stimuli, and in our framework, cartilage can adapt to the adverse mechanical stimuli and re-establish homeostasis. Experiments using a mouse model of disuse of cartilage indicate significant thinning occurs in the first two weeks, followed by stabilization of the thickness in the following four and eight weeks [118]. We thus assumed that the adaptation to pathological loading starts after two weeks, so we chose 0.5 months as our time delay. To fit experimental data from both immobilizing and overloading of human cartilage, we used different temporal averaging periods $\tau^L = 15$ and $\tau^H = 9$ months, respectively. Thus, in our model, human cartilage adapts more quickly to overloading than to immo-

bilizing, consistent with extant experiments. It is worth noting the paucity of experimental data on homeostatic adaptation in cartilage offers a direction to further refine these assumptions.

In Study 2 (§3.2), treatments with suramin showed promising improvements on recovering the thickness of cartilage. Reflecting what we can discern from the literature, our model suggests the degree of recovery depends on the longitudinal intra-tissue mechanics, i.e. on the state of the cartilage as a result of its loading history. In immobilizing, cartilage thinning over 24 months improved from 77% to 82% (for the highest concentration of suramin), while in overloading, the thinning over the same period improved from 95% back to 100%.

Nevertheless in Study 3 (§3.3), the same treatments with suramin after impact injury (i.e. without simultaneous application of active growth factors) showed relatively limited recovery post-injury. In sub-study 1, cartilage thinning over 24 months improved from 74% to 76% (for the highest concentration of suramin applied only during immobilizing). After injury, fewer viable chondrocytes remain and produce proportionally less collagen and proteoglycan. In sub-study 2, we applied the highest concentration of suramin over different time periods of application. For the longest time period of application (i.e. including immobilization for six months and return to normal walking for 18 months), cartilage thinning over 24 months improved from 76% to 77%. This unexpectedly small improvement, relative to what we observed for the same treatment in overloading and immobilizing, motivated us to include treatments with active growth factors in combination with suramin. In sub-study 3, the model showed that constant application of active growth factors, along with suramin (in the highest concentration for the longest time period), resulted in a marked increase in concentration of chondrocytes and greatly improved the recovery from cartilage thinning (i.e. over 24 months the thickness improved from 77% to 87%). These studies demonstrate the potential utility of our framework to test clinical outcomes and guide treatment strategies.

4.2. Modeling framework

Our framework considers cartilage from young, healthy adults; the mean ages were 26 and 37 ± 13.7 years in the two experimental studies we used for calibration, i.e. Frobell [111] and Vanwanseele et al. [110], respectively. The cartilage literature suggests that aging causes abnormal differentiation of chondrocytes that leads to loss of cartilage ECM [119], a factor which we did not consider in the studies presented here. That said, mechanical under- or overuse of cartilage act as non-physiological (pathogenic) stimuli that disrupt homeostasis [119,120], as observed in our studies. Lack of mechanical stimuli can degrade other tissues relevant at the joint scale, e.g. atrophy of bone and muscle due to microgravity during space flights is well-established [121,122], and although we know OA to be a disease of the whole joint, our framework considers only the cartilage tissue.

To establish the mathematical framework for our chemo-mechano-biological model, we simplified complex relationships among chemical species. For example, according to the literature, in human cartilage IL-1 β and TNF- α upregulate ADAMTS-4, but not ADAMTS-5 [78,123,124]; however, in animal models pro-inflammatory cytokines upregulate ADAMTS-5 [125]. For another example, TGF- β is a well known anabolic cytokine in cartilage but in at least one study shows upregulation of ADAMTS-4 [126]. Moreover, mechanical stresses and high levels of TGF- β have been shown to disrupt homeostasis in cartilage [127]. This kind of biological complexity led us to formulate a simplified model capturing the minimally essential functions in a flexible framework. Our mathematical model can be modified or extended based on the availability of data or on a specific question of interest [54,128].

4.3. Model parameters

We used a single set of model parameters in all of our simulations. We estimated the majority of these rate parameters using published estimates of the half-lives of the constituents, cf. (25). We provided rationale for estimating the remaining rate parameters, and we performed numerical experiments to fit experimental measurements of the thickness of cartilage, as quantified using magnetic resonance imaging *in vivo* [110,111].

We expressed the concentration of different chemical species within our mathematical model in a normalized form, which is beneficial to compare simulation results with similar experimental results. The literature reports varying concentrations of chemical species in cartilage among subjects. For example, in synovial fluid the concentration of pro-inflammatory cytokine IL-1 ranges from an average of 0.020 ng/mL in healthy patients [129], to 0.050 ng/mL for patients with mild OA [130], and 0.021 – 0.146 ng/mL for patients with OA [131]. The concentration of latent growth factors (e.g. TGF- β) ranges from 69 to 300 ng/mL across different studies [85,132,133]. Researchers also report variability in concentrations of the latent form of cytokines, but few studies account for concentrations of active forms. Furthermore, many reports of concentrations make no distinction between the active and latent forms of growth factors. With consideration for the variability reported in the literature, we used available data to reasonably bound and estimate the rate parameters.

To demonstrate key features of our coupled modeling framework, we provided representative model parameters, which we estimated based on available, and in some cases sparse, experimental data. Using these parameters, we saw a sudden increase in collagenases in both immobilizing and overloading. During immobilization in particular, the normalized concentration of collagenases increased approximately 9.5 times the normal healthy level in one month, a result which aligns with experimental findings where MMP-3 increased 10 fold in 21 days after immobilization [134].

The increases in collagenases and aggrecanases occur due to the activation of pro-inflammatory cytokines. In our model, the function $f_S(\sigma_1) > 0$ represents the pathological mechanical load required to cause this activation (Fig. 4), and the threshold at which $f_S(\sigma_1)$ is greater than zero (i.e. the threshold of mechanical stimulus required to activate pro-inflammatory cytokines) shifts over time toward a new threshold or homeostatic equilibrium. In contrast, if the value of $f_S(\sigma_1)$ were to remain constant in time, more activated pro-inflammatory cytokines would continue to upregulate more collagenases and aggrecanases, which would cause continued degradation of the matrix and thinning of cartilage without reestablishing a new homeostatic equilibrium.

TIMP is a natural inhibitor of collagenases, and the concentration of TIMP in cartilage depends in part on the concentration of collagenases [83]. Similarly, the concentration of TIMP in cartilage affects the concentration of aggrecanases. In our simulations we observed that higher concentrations of TIMP, conserved by the application of higher concentrations of suramin, inhibited collagenases and aggrecanases (Figs. 7, 8, and 10). Of interest, we see peak values of aggrecanases are less sensitive to suramin compared to the peak values of collagenases. Note that the half-life of aggrecanases is lower than that of collagenases and similar to that of TIMP. Our simulations suggest that in homeostasis the rate of production of aggrecanases is greater than that of collagenases, and has little effect on the concentration of TIMP. Future experiments will help us to validate the impact of suramin on aggrecanases and on cartilage health. Likewise, we can refine the model parameters and framework itself as additional data become available in the future.

4.4. Limitations and outlook

We model cartilage as a non-linear, fiber-reinforced, hyperelastic solid while cartilage is widely considered a fluid-saturated, biphasic material [66]. Our model also simulates cartilage mechanics without considering the osmotic swelling/prestretch within a biphasic model [67] which may affect the growth and remodeling response [135]. The volume of chondrocytes in the superficial and middle zones of cartilage increases with progression of OA, but cells in the deep zone do not change volume [136]. Our framework does not currently distinguish among the different zones.

To establish this initial model we consider only a subset of known signaling pathways while many more exist [137]. We also assume only chondrocytes produce cytokines and enzymes, while fibroblasts and macrophages express many of the pro-inflammatory cytokines, collagenases, and aggrecanases that contribute to degradation of cartilage [138]. We combine chemical species into classes based on their general roles in cartilage, although not all species within each class have identical effects on cartilage homeostasis. Moreover we estimate the half-lives for these classes of chemical species despite variability in the half-lives within each class. Anabolic cytokines and growth factors have different half-lives: e.g. the half-lives of BMP, FGF, and TGF- β 1 are 0.12 – 0.27, 4 – 13, and 1.67 h, respectively [102–104]. Different pro-inflammatory cytokines have different half-lives, too: e.g. the half-lives of TNF- α , IL-6, IL-1 α and IL-1 β are 0.08, 1, 15, and 2.5 h, respectively [101,105,106]. The half-lives of MMP-1 and MMP-3 are 210 h and 4 h, respectively [117]. Furthermore, the relative proportion of these chemical species in cartilage is unknown; with more data, we can refine model parameters or extend the model itself.

We calibrated our coupled chemo-mechano-biological model of evolving osteoarthritis in cartilage using two longitudinal experimental studies, which measure the thickness of cartilage. Our mechanical stimulus functions assume that pathological maximum shear stresses convert latent growth factors to their active forms, while first principal stresses convert latent cytokines to their active forms. Additional experiments and simulations with realistic geometries and mechanical loads will clarify differences in how intra-tissue mechanics drive the up- and down-regulation of chemical species. Longitudinal quantification of biochemical constituents in evolving cartilage is not yet available in literature; future studies of this nature, both *in vitro* and *in vivo*, will allow us and others to refine this model.

We present a novel mathematical framework incorporating the coupled longitudinal evolution of key chemical, structural, and bio-

logical constituents of cartilage and exercise our model to demonstrate thinning of cartilage that leads to the progression of OA. Our proposed model is a first step towards investigating the biochemical, mechanical, and biological evolution of cartilage and chondrocytes in degeneration or progression of OA, as well as the respective responses to pharmacological interventions and therapies. With more longitudinal experimental data on chemical species, our mathematical model can be fitted to predict clinical outcomes. To exercise our model we demonstrated a possible treatment for cartilage thinning that progressively leads to OA. In recent animal studies suramin showed chondroprotective properties by decreasing aggrecanases and collagenases, and increasing TIMP [139], which we observe in Figs. 7, 8, and 10. We aim to implement our chemo-mechano-biological framework for finite element analyses, thus enabling advanced understanding of patient-specific pathological changes due to biomechanical factors, improved clinical diagnostics and therapies [43], and new methods for non-invasive diagnosis and pre-/post-operative decision making. Leveraging our framework in future studies will enable us to link physical activity, and the resulting mechanical stimuli, to the progression of OA and loss of cartilage function, enabling new fundamental understanding of the complex progression of OA, and elucidating new perspectives on causes, treatments, and possible preventions.

Statements of Ethical Approval

The authors do not need ethical approval.

Funding

US National Science Foundation (NSF) 1662429. PNW acknowledges partial support from UK Engineering and Physical Sciences Research Council (EPSRC) EP/N014642/1 and EP/T017899/1.

Declaration of Competing Interest

The authors declare no competing interests.

Appendix A

Deformation gradients describing transversely anisotropic growth take the general form,

$$\mathbf{F}^g = \alpha \mathbf{I} + \beta \mathbf{n} \otimes \mathbf{n}, \quad (\text{A.1})$$

where α and β are parameters controlling the growth kinematics. To prescribe isotropic volume growth (IVG) $\alpha = \hat{v}^{1/3}$ and

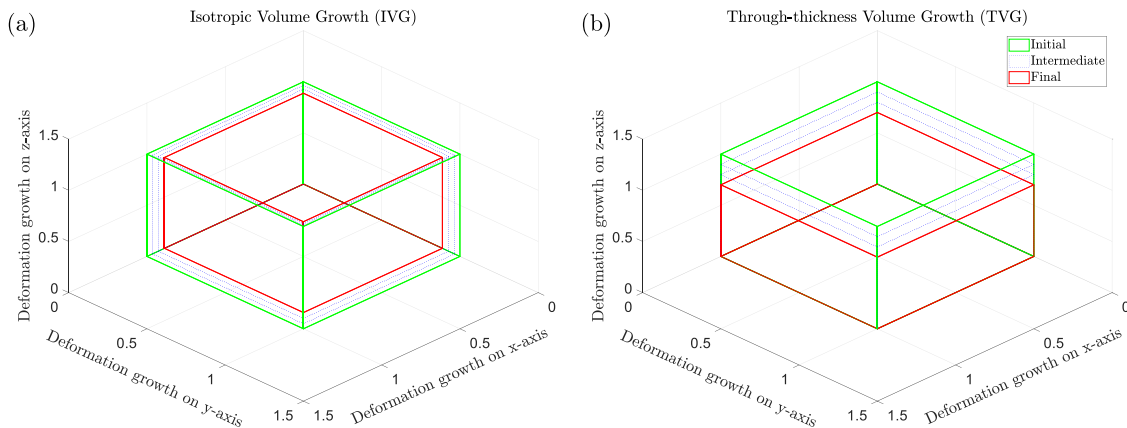


Fig. A1. Representative kinematics of (a) isotropic volume growth (IVG) and (b) through-thickness volume growth (TVG) with $\mathbf{F}^e = \mathbf{I}$ and $\hat{v} \in [1, 0.7]$ (negative growth). In IVG the volume shrinks equally in all directions. In TVG, the volume shrinks only in the through-thickness ($\mathbf{n} = [0\ 0\ 1]^T$) direction. Solid green ($\hat{v} = 1$) and red ($\hat{v} = 0.7$) outline the initial and final configurations, respectively, while dotted blue outlines represent intermediate configurations. (For interpretation of the references to colour in this figure legend, the reader is referred to the web version of this article.)

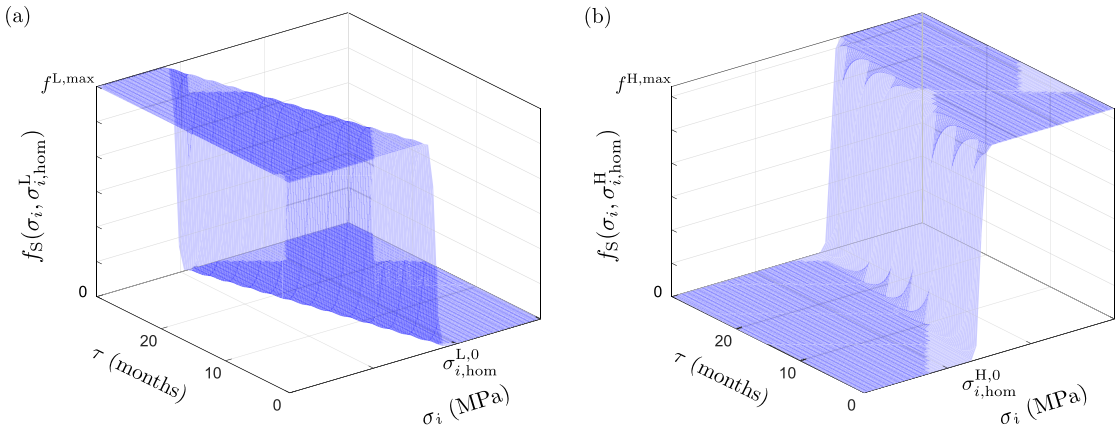


Fig. B.1. Mechanical stimuli activates latent cytokines and growth factors that are a function of stress and time τ . Representative $f_S(\sigma_i, \sigma_{i,hom}^L, \sigma_{i,hom}^H)$ for pathological loading conditions, which is a function of $\sigma_i(\tau)$, $\sigma_{i,hom}^L$, and $\sigma_{i,hom}^H$. Initially, at $\tau = 0$ the lower homeostatic threshold is $\sigma_{i,hom}^{L,0}$. As τ increases, chondrocytes adapt the pathological stress σ_{sh} , and $\sigma_{i,hom}^L$ shifts linearly: (a) represents immobilizing, where $\sigma_{i,hom}^L$ decreases, and (b) represents overloading, where $\sigma_{i,hom}^H$ increases.

$\beta = 0$. However, by specifying $\alpha = 1$ and $\beta = \hat{v} - 1$ we introduce TVG which captures the degradation of cartilage in the through-thickness direction, cf. (1). In Fig. A1 we illustrate the kinematics of IVG and TVG using the same total volume loss. We observe that the change of volume occurs in all directions equally in IVG while the change of volume occurs only in the through-thickness direction in TVG.

Appendix B

In Fig. B.1 we illustrate the mathematics of homeostatic adaptation to mechanical stimuli.

Appendix C

In Figs. C.1 and C.2 we complete a representative parameter study of the time averaging period τ^L during immobilizing, and illustrate the evolution of both intra-tissue mechanics and of cellular and molecular species, respectively.

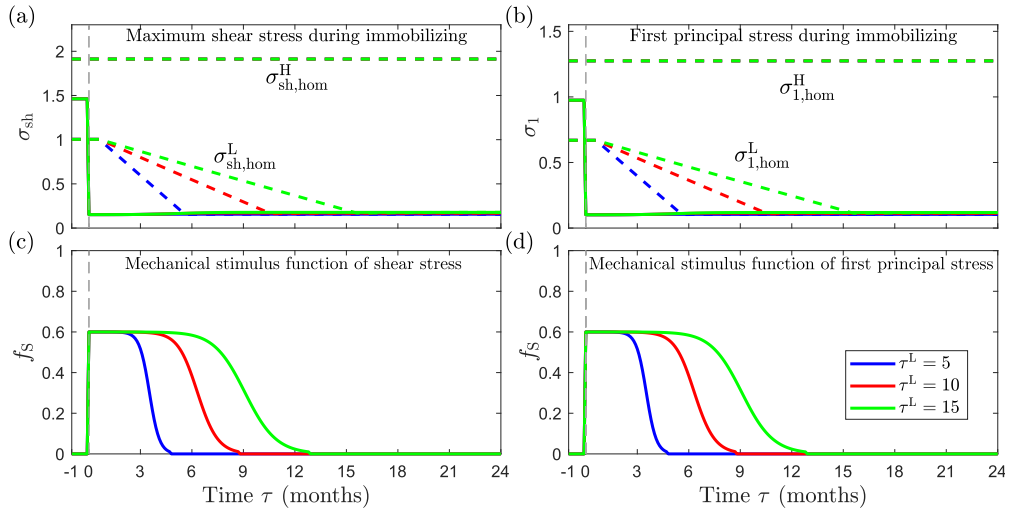


Fig. C.1. Evolution of intra-tissue mechanics while cartilage evolves in immobilizing with different time averaging periods τ^L . Blue, red, and green curves represent $\tau^L = 5, 10$, and 15 , respectively. Specifically: (a) maximum shear stress σ_{sh} during immobilizing, (b) first principal stress σ_1 during immobilizing, (c) mechanical stimulus functions of shear stress f_S , and (d) mechanical stimulus functions of first principal stress f_S . (For interpretation of the references to colour in this figure legend, the reader is referred to the web version of this article.)

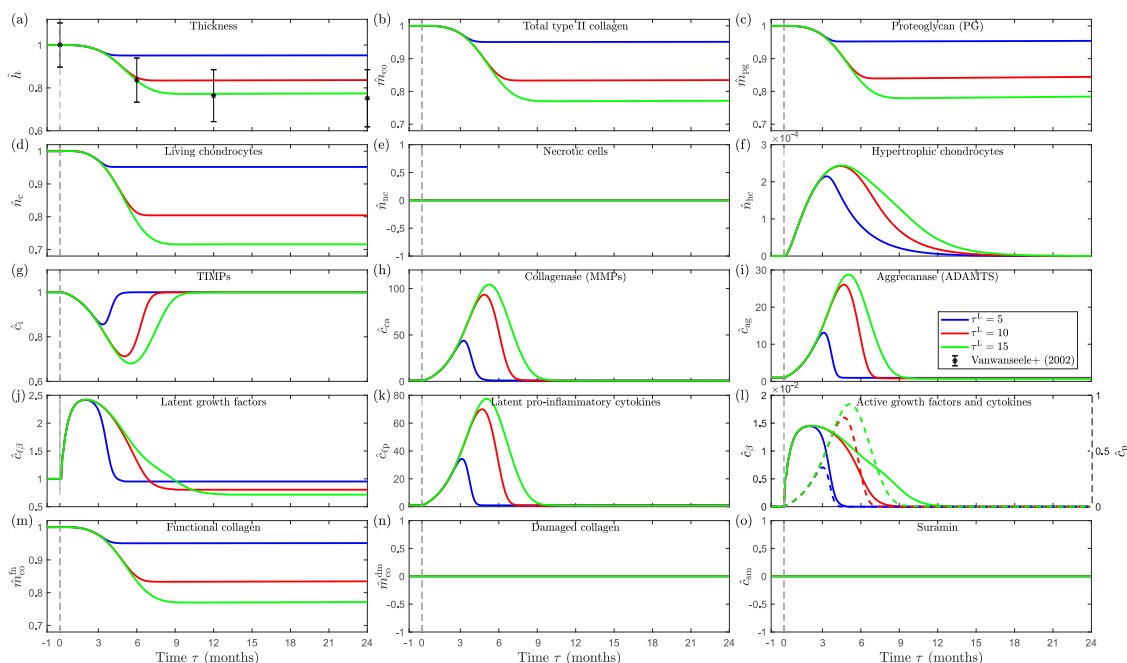


Fig. C.2. Cartilage evolves in immobilizing with different time averaging periods τ^L . Blue, red, and green curves represent $\tau^L = 5, 10$, and 15 , respectively. Time $\tau < 0$ months represents healthy homeostatic conditions, and immobilizing starts at $\tau = 0$ months. With $\tau^L = 15$ months, thickness of cartilage matches with the experimental data from Vanwanseele et al. [110]. See Table 1 for a description of the variables. (For interpretation of the references to colour in this figure legend, the reader is referred to the web version of this article.)

References

- R.F. Loeser, S.R. Goldring, C.R. Scanzello, M.B. Goldring, Osteoarthritis: a disease of the joint as an organ, *Arthritis Rheum.* 64 (2012) 1697–1707.
- R.C. Lawrence, D.T. Felson, C.G. Helmick, L.M. Arnold, H. Choi, R.A. Deyo, S. Gabriel, R. Hirsch, M.C. Hochberg, G.G. Hunder, J.M. Jordan, J.N. Katz, H.M. Kremers, F. Wolfe, Estimates of the prevalence of arthritis and other rheumatic conditions in the United States: Part II, *Arthritis Rheum.* 58 (2008) 26–35.
- S. Grässel, D. Muschler, Recent advances in the treatment of osteoarthritis [version 1; peer review: 3 approved], *F1000Research* 9 (2020).
- V.C. Mow, R. Huiskes, Structure and function of ligaments and tendons, in: S.L.-Y. Woo, T.Q. Lee, S.D. Abramowitch, T.W. Gilbert (Eds.), *Basic Orthopaedic Biomechanics and Mechano-Biology*, Lippincott Williams & Wilkins, Philadelphia, 2005, pp. 301–342.
- N.D. Broom, D.L. Marra, Ultrastructural evidence for fibril-to-fibril associations in articular cartilage and their functional implication, *J. Anat.* 146 (1986) 185–200.
- W.B. Zhu, V.C. Mow, T.J. Koob, D.R. Eyre, Viscoelastic shear properties of articular cartilage and the effects of glycosidase treatments, *J. Orthop. Res.* 11 (1993) 771–781.
- M.B. Goldring, K.B. Marcu, Cartilage homeostasis in health and rheumatic diseases, *Arthritis Res. Ther.* 11 (2009) 224. PMC2714092
- C. Chen, D.T. Tambe, L. Deng, L. Yang, Biomechanical properties and mechanobiology of the articular chondrocyte, *Am. J. Physiol. Cell Physiol.* 305 (2013) C1202–C1208.
- J.P.G. Urban, The chondrocyte: a cell under pressure, *Rheumatology* 33 (1994) 901–908.
- R.L. Smith, J. Lin, M.C.D. Trindade, J. Shida, G. Kajiyama, T. Vu, A.R. Hoffman, M.C.H. van der Meulen, S.B. Goodman, D.J. Schurman, D.R. Carter, Time-dependent effects of intermittent hydrostatic pressure on articular chondrocyte type II collagen and aggrecan mRNA expression, *J. Radiat. Res. Dev.* 37 (2000).
- S.D. Waldman, C.G. Spiteri, M.D. Grynpas, R.M. Pilliar, J. Hong, R.A. Kandel, Effect of biomechanical conditioning on cartilaginous tissue formation in vitro, *J. Bone Joint Surg.* 85 (2003) 101–105.
- M. Wong, M. Siegrist, K. Goodwin, Cyclic tensile strain and cyclic hydrostatic pressure differentially regulate expression of hypertrophic markers in primary chondrocytes, *Bone* 33 (2003) 685–693.
- J.A. Buckwalter, H.J. Mankin, A.J. Grodzinsky, Articular cartilage and osteoarthritis, in: V.D. Pellegrini (Ed.), *AAOS Instructional Course Lectures*, Vol. 54, American Academy of Orthopaedic Surgeons, Rosemont, IL, 2005, pp. 465–480.
- K. Honda, S. Ohno, K. Tanimoto, C. Ijuin, N. Tanaka, T. Doi, Y. Kato, K. Tanne, The effects of high magnitude cyclic tensile load on cartilage matrix metabolism in cultured chondrocytes, *Eur. J. Cell Biol.* 79 (2000) 601–609.
- C.J. Hunter, S.M. Imler, P. Malaviya, R.M. Nerem, M.E. Levenston, Mechanical compression alters gene expression and extracellular matrix synthesis by chondrocytes cultured in collagen I gels, *Biomaterials* 23 (2002) 1249–1259.
- Z. Peng, H. Sun, V. Bunpetch, Y. Koh, Y. Wen, D. Wu, H. Ouyang, The regulation of cartilage extracellular matrix homeostasis in joint cartilage degeneration and regeneration, *Biomaterials* 26 (2005) 120555.
- L.C. Tetlow, D.J. Adlam, D.E. Woolley, Matrix metalloproteinase and proinflammatory cytokine production by chondrocytes of human osteoarthritic cartilage: associations with degenerative changes, *Arthritis Rheum.* 44 (2001) 585–594.
- S. Pérez-García, M. Carrión, I. Gutiérrez-Cañas, R. Villanueva-Romero, D. Castro, C. Martínez, I. González-Álvaro, F.J. Blanco, Y. Juarranz, R.P. Gomariz, Profile of matrix-remodeling proteinases in osteoarthritis: impact of fibronectin, *Cells* 9 (2019) 40.
- E. Charlier, B. Relic, C. Deroyer, O. Malaise, S. Neuville, J. Collée, M. Malaise, D. De Seny, Insights on molecular mechanisms of chondrocytes death in osteoarthritis, *Int. J. Mol. Sci.* 17 (2016) 2146.
- L.J. Sandell, T. Aigner, Articular cartilage and changes in arthritis. an introduction: cell biology of osteoarthritis, *Arthritis Res.* 3 (2001) 107–113.
- M.B. Goldring, The role of the chondrocyte in osteoarthritis, *Arthritis Rheum.* 43 (2000) 1916–1926.
- T. Aigner, B. Kurz, N. Fukui, L. Sandell, Roles of chondrocytes in the pathogenesis of osteoarthritis, *Curr. Opin. Rheumatol.* 14 (2002) 578–584.
- T. Tallheden, C. Bengtsson, C. Brantsing, E. Sjögren-Jansson, L. Carlsson, L. Petersson, M. Brittberg, A. Lindahl, Proliferation and differentiation potential of chondrocytes from osteoarthritic patients, *Arthritis Res. Ther.* 7 (2005) R560–R568.
- K.P.H. Pritzker, S. Gay, S.A. Jimenez, K. Ostergaard, J.P. Pelletier, P.A. Revell, D. Salter, W.B. van den Berg, Osteoarthritis cartilage histopathology: grading and staging, *Osteoarthritis Cartilage* 14 (2006) 13–29.
- T. Aigner, S. Söder, P.M. Gebhard, A. McAlinden, J. Haag, Mechanisms of disease: role of chondrocytes in the pathogenesis of osteoarthritis—structure, chaos and senescence, *Nat. Rev. Rheumatol.* 3 (2007) 391–399.
- S. Hashimoto, R.L. Ochs, S. Komiya, M. Lotz, Linkage of chondrocyte apoptosis and cartilage degradation in human osteoarthritis, *Arthritis Rheum.* 41 (1998) 1632–1638.
- S. Hashimoto, K. Takahashi, D. Amiel, R.D. Coutts, M. Lotz, Chondrocyte apoptosis and nitric oxide production during experimentally induced osteoarthritis, *Arthritis Rheum.* 41 (1998) 1266–1274.
- M. Lotz, S. Hashimoto, K. Kühn, Mechanisms of chondrocyte apoptosis, *Osteoarthritis Cartilage* 7 (1999) 389–391.
- H.A. Kim, Y.J. Lee, S.C. Seong, K.W. Choe, Y.W. Song, Apoptotic chondrocyte death in human osteoarthritis, *J. Rheumatol.* 27 (2000) 455–462.
- J.P. Pelletier, D.V. Jovanovic, V.L. Coman, J.C. Fernandes, P.T. Manning, J.R. Conner, M.G. Currie, J.M. Pelletier, Selective inhibition of inducible nitric oxide synthase reduces progression of experimental osteoarthritis *in vivo*: possible link with the reduction in chondrocyte apoptosis and caspase 3 level, *Arthritis Rheum.* 43 (2000) 1290–1299.

[31] D.Y. Kim, H.W. Taylor, R.M. Moore, D.B. Paulsen, D.Y. Cho, Articular chondrocyte apoptosis in equine osteoarthritis, *Vet. J.* 166 (2003) 52–57.

[32] D. Mistry, Y. Oue, M.G. Chambers, M.V. Kayser, R.M. Mason, Chondrocyte death during murine osteoarthritis, *Osteoarthritis Cartilage* 12 (2004) 131–141.

[33] C.M. Thomas, C.J. Fuller, C.E. Whittles, M. Sharif, Chondrocyte death by apoptosis is associated with cartilage matrix degradation, *Osteoarthritis Cartilage* 15 (2007) 27–34.

[34] Z. Zamli, M. Sharif, Chondrocyte apoptosis: a cause or consequence of osteoarthritis? *Int. J. Rheum. Dis.* 14 (2011) 159–166.

[35] F.J. Blanco, R. Guitian, E.V. Martul, F.J. de Toro, F. Galdo, Osteoarthritis chondrocytes die by apoptosis: a possible pathway for osteoarthritis pathology, *Arthritis Rheum.* 41 (1998) 284–289.

[36] F. Héraud, A. Héraud, M.F. Harmand, Apoptosis in normal and osteoarthritic human articular cartilage, *Ann. Rheum. Dis.* 59 (2000) 959–965.

[37] J.B. Kouri, J.M. Aguilar, J. Reyes, K.A. Lozoya, S. González, Apoptotic chondrocytes from osteoarthritic human articular cartilage and abnormal calcification of subchondral bone, *J. Rheumatol.* 27 (2000) 1005–1019.

[38] M. Sharif, A. Whitehouse, P. Sharman, M. Perry, M. Adams, Increased apoptosis in human osteoarthritic cartilage corresponds to reduced cell density and expression of caspase-3, *Arthritis Rheum.* 50 (2004) 507–515.

[39] L.A. Fortier, J.U. Barker, E.J. Strauss, T.M. McCarrel, B.J. Cole, The role of growth factors in cartilage repair, *Clin. Orthop. Relat. Res.* 469 (2011) 2706–2715.

[40] C.-W. Su, C.-W. Lin, W.-E. Yang, S.-F. Yang, TIMP-3 as a therapeutic target for cancer, *Ther. Adv. Med. Oncol.* 11 (2019) 1–17.

[41] D. Fan, Z. Kassiri, Biology of tissue inhibitor of metalloproteinase 3 (TIMP3), and its therapeutic implications in cardiovascular pathology, *Front. Physiol.* 11 (2020) 1–16.

[42] M. Kashiwagi, M. Tortorella, H. Nagase, K. Brew, TIMP-3 is a potent inhibitor of aggrecanase 1 (ADAM-TS4) and aggrecanase 2 (ADAM-TS5), *J. Biol. Chem.* 276 (2001) 12501–12504.

[43] H. Nakamura, P. Vo, I. Kanakis, K. Liu, G. Bou-Gharios, Aggrecanase-selective tissue inhibitor of metalloproteinase-3 (TIMP3) protects articular cartilage in a surgical mouse model of osteoarthritis, *Sci. Rep.* 10 (2020) 9288.

[44] N. Wiedemer, D.A. Hauser, P. Mäser, 100 Years of suramin, *Antimicrob. Agents Chemother.* 64 (2020).

[45] R.K. Naviaux, B. Curtis, K. Li, J.C. Naviaux, A.T. Bright, G.E. Reiner, M. Westerfield, S. Goh, W.A. Alaynick, L. Wang, E.V. Capparelli, C. Adams, J. Sun, S. Jain, F. He, D.A. Arellano, L.E. Mash, L. Chukoskie, A. Lincoln, J. Townsend, Low-dose suramin in autism spectrum disorder: a small, phase I/II, randomized clinical trial, *Ann. Clin. Transl. Neurol.* 4 (2017) 491–505.

[46] A. Chanalaris, C. Doherty, B.D. Marsden, G. Cambridge, S.P. Wren, H. Nagase, L. Troeberg, Suramin inhibits osteoarthritic cartilage degradation by increasing extracellular levels of chondroprotective tissue inhibitor of metalloproteinases 3, *Mol. Pharmacol.* 92 (2017) 459–468.

[47] N.S. Landinez-Parra, D.A. Garzón-Alvaredo, J.C. Vanegas-Acosta, A phenomenological mathematical model of the articular cartilage damage, *Comput. Methods Programs Biomed.* 104 (2011) e58–e74.

[48] S.M. Hosseini, W. Wilson, K. Ito, C.C. Van Donkelaar, A numerical model to study mechanically induced initiation and progression of damage in articular cartilage, *Osteoarthritis Cartilage* 22 (2014) 95–103.

[49] M.K. Liukkonen, M.E. Mononen, O. Klets, J.P. Arokoski, S. Saarakkala, R.K. Korhonen, Simulation of subject-specific progression of knee osteoarthritis and comparison to experimental follow-up data: data from the osteoarthritis initiative, *Sci. Rep.* 7 (2017) 1–14.

[50] M.E. Mononen, M.K. Liukkonen, R.K. Korhonen, Utilizing atlas-based modeling to predict knee joint cartilage degeneration: data from the osteoarthritis initiative, *Ann. Biomed. Eng.* 47 (2019) 813–825.

[51] G.I. Kapitanov, X. Wang, B.P. Ayati, M.J. Brouillette, J.A. Martin, Linking cellular and mechanical processes in articular cartilage lesion formation: a mathematical model, *Front. Bioeng. Biotechnol.* 4 (2016).

[52] G.A. Orozco, P. Tanska, C. Florea, A.J. Grodzinsky, R.K. Korhonen, A novel mechanobiological model can predict how physiologically relevant dynamic loading causes proteoglycan loss in mechanically injured articular cartilage, *Sci. Rep.* 8 (2018) 15599.

[53] A.S. Eskelinen, P. Tanska, C. Florea, G.A. Orozco, P. Julkunen, A.J. Grodzinsky, R.K. Korhonen, Mechanobiological model for simulation of injured cartilage degradation via proinflammatory cytokines and mechanical, *PLoS Comput. Biol.* 16 (2020) 1–25.

[54] M. Segarra-Queralt, G. Piella, J. Noaill, Network-based modelling of mechano-inflammatory chondrocyte regulation in early osteoarthritis, *Front. Bioeng. Biotechnol.* 11 (2023) 1–17.

[55] J.D. Humphrey, K.R. Rajagopal, A constrained mixture model for growth and remodeling of soft tissues, *Math. Model. Meth. Appl. Sci.* 12 (2002) 407–430.

[56] A. Grytsan, T.S.E. Eriksson, P.N. Watton, T.C. Gasser, Growth description for vessel wall adaptation: a thick-walled mixture model of abdominal aortic aneurysm evolution, *Materials* 10 (2017) 1–19.

[57] D. Ambrosi, M. Ben Amar, C.J. Cyron, A. DeSimone, A. Goriely, J.D. Humphrey, E. Kuhl, Growth and remodelling of living tissues: perspectives, challenges and opportunities, *J. R. Soc. Interface* 16 (2019) 20190233.

[58] L. Lamm, H. Holthusen, T. Brepols, S. Jockenhövel, S. Reese, A macroscopic approach for stress-driven anisotropic growth in bioengineered soft tissues, *Biomech. Model. Mechanobiol.* 21 (2022) 627–645.

[59] X. Zhan, X.Y. Luo, Volumetric growth of soft tissues evaluated in the current configuration, *Biomech. Model. Mechanobiol.* 21 (2022) 569–588.

[60] A. Davol, M.S. Bingham, R.L. Sah, S.M. Kirsch, A nonlinear finite element model of cartilage growth, *Biomech. Model. Mechanobiol.* 7 (2008) 295–307.

[61] C. Bandeiras, A. Completo, A mathematical model of tissue-engineered cartilage development under cyclic compressive loading, *Biomech. Model. Mechanobiol.* 16 (2017) 651–666.

[62] M. Baker, B.S. Brook, M.R. Owen, Mathematical modelling of cytokines, MMPs and fibronectin fragments in osteoarthritic cartilage, *J. Math. Biol.* 75 (2017) 985–1024.

[63] N. Moise, A. Friedman, Rheumatoid arthritis - a mathematical model, *J. Theor. Biol.* 461 (2019) 17–33.

[64] V.D. Sree, A.B. Tepole, Computational systems mechanobiology of growth and remodeling: integration of tissue mechanics and cell regulatory network dynamics, *Curr. Opin. Biomed. Eng.* 15 (2020) 75–80.

[65] P. Aparicio, M.S. Thompson, P.N. Watton, A novel chemo-mechano-biological model of arterial tissue growth and remodelling, *J. Biomech.* 49 (2016) 2321–2330.

[66] D.M. Pierce, M.J. Unterberger, W. Trobin, T. Ricken, G.A. Holzapfel, A microstructurally based continuum model of cartilage viscoelasticity and permeability incorporating statistical fiber orientation, *Biomech. Model. Mechanobiol.* 15 (2016) 229–244.

[67] X. Wang, T.S.E. Eriksson, T. Ricken, D.M. Pierce, On incorporating osmotic pre-stretch/prestress in image-driven finite element simulations of cartilage, *J. Mech. Behav. Biomed. Mat.* 86 (2018) 409–422.

[68] G.A. Holzapfel, *Nonlinear Solid Mechanics: A Continuum Approach for Engineering*, Wiley, 2000.

[69] P. Bažant, B.H. Oh, Efficient numerical integration on the surface of a sphere, *Z. Angew. Math. Mech.* 66 (1986) 37–49.

[70] M. Rahmati, G. Nalesto, A. Mobasher, M. Mozafari, Aging and osteoarthritis: central role of the extracellular matrix, *Ageing Res. Rev.* 40 (2017) 20–30.

[71] T. Tallheden, C. Bengtsson, C. Brantsing, E. Sjögren-Jansson, L. Carlsson, L. Petersson, M. Brittberg, A. Lindahl, Proliferation and differentiation potential of chondrocytes from osteoarthritic patients, *Arthritis Res. Ther.* 7 (2005).

[72] X. Houard, M.B. Goldring, F. Berenbaum, Homeostatic mechanisms in articular cartilage and role of inflammation in osteoarthritis, *Curr. Rheumatol. Rep.* 15 (2013).

[73] W. Madej, A. van Caam, E.N. Blaney Davidson, P.M. van der Kraan, P. Buma, Physiological and excessive mechanical compression of articular cartilage activates Smad2/3P signaling, *Osteoarthritis Cartilage* 22 (2014) 1018–1025.

[74] A.J. Schuerwagh, E.J. Dombrecht, W.J. Stevens, J.F. Van Offel, C.H. Brdits, L.S. De Clerck, Influence of pro-inflammatory (IL-1 α , IL-6, TNF- α , IFN- γ) and anti-inflammatory (IL-4) cytokines on chondrocyte function, *Osteoarthritis Cartilage* 11 (2003) 681–687.

[75] P.F. Argote, J.T. Kaplan, A. Poon, X. Xu, L. Cai, N.C. Emery, D.M. Pierce, C.P. Neu, Chondrocyte viability is lost during high-rate impact loading by transfer of amplified strain, but not stress, to pericellular and cellular regions, *Osteoarthritis Cartilage* 27 (2019) 1822–1830.

[76] A.J. Sophia Fox, A. Bedi, S.A. Rodeo, The basic science of articular cartilage: structure, composition, and function, *Sports Health* 1 (2009) 461–468.

[77] E.-S.E. Mehana, A.F. Khafaga, S.S. El-Blehi, The role of matrix metalloproteinases in osteoarthritis pathogenesis: an updated review, *Life Sci.* 234 (2019) 116786.

[78] P. Verma, K. Dalal, ADAMTS-4 and ADAMTS-5: key enzymes in osteoarthritis, *J. Cell Biochem.* 112 (2011) 3507–3514.

[79] M.B. Goldring, M. Otero, D.A. Plumb, C. Dragomir, M. Favero, K. El Hachem, K. Hashimoto, H.I. Roach, E. Olivotto, R.M. Borzì, K.B. Marcu, Roles of inflammatory and anabolic cytokines in cartilage metabolism: signals and multiple effectors converge upon MMP-13 regulation in osteoarthritis, *Eur. Cell Mater.* 21 (2011) 202–220.

[80] A.E.M. Jorgensen, M. Kjær, K.M. Heinemeier, The effect of aging and mechanical loading on the metabolism of articular cartilage, *J. Rheumatol.* 44 (2017) 410–417.

[81] N.G.M. Thielen, P.M. van der Kraan, A.P.M. van Caam, TGF β /BMP signaling pathway in cartilage homeostasis, *Cells* 8 (2019) 969.

[82] P.M. Van der Kraan, W.B. Van den Berg, Chondrocyte hypertrophy and osteoarthritis: role in initiation and progression of cartilage degeneration? *Osteoarthritis Cartilage* 20 (2012) 223–232.

[83] K. Yamamoto, D. Wilkinson, G. Bou-Gharios, Targeting dysregulation of metalloproteinase activity in osteoarthritis, *Calciif. Tissue Int.* 109 (2021) 277–290.

[84] M. Hyttinen, C. Penttinen, J. Keski-Oja, Latent TGF- β binding proteins: extracellular matrix association and roles in TGF- β activation, *Crit. Rev. Clin. Lab. Sci.* 41 (2004) 233–264.

[85] M.B. Albro, R.J. Nims, A.D. Cigan, K.J. Yeroushalmi, T. Alliston, C.T. Hung, G.A. Ateshian, Accumulation of exogenous activated TGF- β in the superficial zone of articular cartilage, *Biophys. J.* 104 (2013) 1794–1804.

[86] C.P. Neu, A. Khalafi, K. Komvopoulos, T.M. Schmid, A.H. Reddi, Mechanotransduction of bovine articular cartilage superficial zone protein by transforming growth factor β signaling, *Arthritis Rheum.* 56 (2007) 3706–3714.

[87] M.B. Albro, A.D. Cigan, R.J. Nims, K.J. Yeroushalmi, S.R. Oungoulian, C.T. Hung, G.A. Ateshian, Shearing of synovial fluid activates latent TGF- β , *Osteoarthritis Cartilage* 20 (2012) 1374–1382.

[88] P. Wojdasiewicz, Ł.A. Poniatowski, D. Szukiewicz, The role of inflammatory and anti-inflammatory cytokines in the pathogenesis of osteoarthritis, *Mediators Inflamm.* 2014 (2014) 561459.

[89] M. Anghelina, D. Sjöstrom, P. Perera, J. Nam, T. Knobloch, S. Agarwal, Regulation of biomechanical signals by NF- κ B transcription factors in chondrocytes, *Biorheology* 45 (2008) 245–256.

[90] K.B. Marcu, M. Otero, E. Olivotto, R.M. Borzi, M.B. Goldring, NF- κ B signaling: multiple angles to target OA, *Curr. Drug Targets* 11 (2010) 599–613.

[91] T.L. Vincent, A.K.T. Wann, Mechanoadaptation: articular cartilage through thick and thin, *J. Physiol.* 597 (2019) 1271–1281.

[92] P. Aparicio, A. Mandaltsi, J. Boamah, H. Chen, A. Selimovic, M. Bratby, R. Uberoi, Y. Ventikos, P. Watton, Modelling the influence of endothelial heterogeneity on the progression of arterial disease: application to abdominal aortic aneurysm evolution, *Int. J. Numer. Meth. Biomed. Eng.* 30 (2014) 563–586.

[93] J.T. Kaplan, C.P. Neu, H. Drissi, N.C. Emery, D.M. Pierce, Cyclic loading of human articular cartilage: the transition from compaction to fatigue, *J. Mech. Behav. Biomed. Mat.* 65 (2017) 734–742.

[94] S.C. Walpole, D. Prieto-Merino, P. Edwards, J. Cleland, G. Stevens, I. Roberts, The weight of nations: an estimation of adult human biomass, *BMC Public Health* 12 (2012) 1–6.

[95] M.S. Kuster, G.A. Wood, G.W. Stachowiak, A. Gachter, Joint load considerations in total knee replacement, *J. Bone Joint Surg.* 79 (1997) 109–113.

[96] D.M. Pierce, T. Ricken, G.A. Holzapfel, A hyperelastic biphasic fiber-reinforced model of articular cartilage considering distributed collagen fiber orientations: continuum basis, computational aspects and applications, *Comput. Methods Biomed. Eng.* 16 (2013) 1344–1361.

[97] H.A. Kim, Y.W. Song, Apoptotic chondrocyte death in rheumatoid arthritis, *Arthritis Rheum.* 42 (1999) 1528–1537.

[98] N. Verzijl, J. DeGroot, S.R. Thorpe, R.A. Bank, J.N. Shaw, T.J. Lyons, J.W. Bijlsma, F.P. Lafeber, J.W. Baynes, J.M. Tekkopeele, Effect of collagen turnover on the accumulation of advanced glycation end products, *J. Biol. Chem.* 275 (2000) 39027–39031.

[99] A. Maroudas, M.T. Bayliss, N. Uchitel-Kaushansky, R. Schneiderman, E. Gilav, Aggrecan turnover in human articular cartilage: use of aspartic acid racemization as a marker of molecular age, *Arch. Biochem. Biophys.* 350 (1998) 61–71.

[100] C.B. Little, C.T. Meeker, S.B. Golub, K.E. Lawlor, P.J. Farmer, S.M. Smith, A.J. Fosang, Blocking aggrecanase cleavage in the aggrecan interglobular domain abrogates cartilage erosion and promotes cartilage repair, *J. Clin. Invest.* 117 (2007) 1627–1636.

[101] D.J. Hazuda, J.C. Lee, P.R. Young, The kinetics of interleukin 1 secretion from activated monocytes. Differences between interleukin 1 α and interleukin 1 β , *J. Biol. Chem.* 263 (1988) 8473–8479.

[102] L.M. Wakefield, T.S. Winokur, R.S. Hollands, K. Christopherson, A.D. Levinson, M.B. Sporn, Recombinant latent transforming growth factor beta 1 has a longer plasma half-life in rats than active transforming growth factor beta 1, and a different tissue distribution, *J. Clin. Invest.* 86 (1990) 1976–1984.

[103] A.R. Poynton, J.M. Lane, Safety profile for the clinical use of bone morphogenetic proteins in the spine, *Spine* 27 (2002) 40–48.

[104] T. Shiba, D. Nishimura, Y. Kawazoe, Y. Onodera, K. Tsutsumi, R. Nakamura, M. Ohshiro, Modulation of mitogenic activity of fibroblast growth factors by inorganic polyphosphate, *J. Biol. Chem.* 278 (2003) 26788–26792.

[105] R. Mehra, A. Storfer-Isser, H.L. Kirchner, N. Johnson, N. Jenny, R.P. Tracy, S. Redline, Soluble interleukin 6 receptor: a novel marker of moderate to severe sleep-related breathing disorder, *Arch. Intern. Med.* 166 (2006) 1725–1731.

[106] R. Simó, A. Barbosa-Desouges, A. Lecube, C. Hernandez, D.M. Selva, Potential role of tumor necrosis factor- α in downregulating sex hormone-binding globulin, *Diabetes* 61 (2012) 372–382.

[107] K. Yamamoto, K. Owen, A.E. Parker, S.D. Scilabre, J. Duhdia, D.K. Strickland, L. Troeberg, H. Nagase, Low density lipoprotein receptor-related protein 1 (LRP1)-mediated endocytic clearance of a disintegrin and metalloproteinase with thrombospondin motifs-4 (adams-4): functional differences of non-catalytic domains of adams-4 and adams-5 in lrp1 binding*, *J. Bio. Chem.* 289 (2014) 6462–6474.

[108] C.M. Doherty, R. Visse, D. Dinakarpandian, D.K. Strickland, H. Nagase, L. Troeberg, Engineered tissue inhibitor of metalloproteinases-3 variants resistant to endocytosis have prolonged chondroprotective activity, *J. Bio. Chem.* 291 (2016) 22160–22172.

[109] R. Dreier, Hypertrophic differentiation of chondrocytes in osteoarthritis: the developmental aspect of degenerative joint disorders, *Arthritis Res. Ther.* 12 (2010) 216, doi:10.1186/ar3117.

[110] B. Vanwanseele, F. Eckstein, H. Knecht, E. Stüssi, A. Spaepen, Knee cartilage of spinal cord-injured patients displays progressive thinning in the absence of normal joint loading and movement, *Arthritis Rheum.* 46 (2002) 2073–2078.

[111] R.B. Frobell, Change in cartilage thickness, posttraumatic bone marrow lesions, and joint fluid volumes after acute ACL disruption: a two-year prospective MRI study of sixty-one subjects, *J. Bone Joint Surg.* 93 (2011) 1096–1103.

[112] E.N. Blaney Davidson, P.M. van der Kraan, W.B. van den Berg, TGF- β and osteoarthritis, *Osteoarthritis Cartilage* 15 (2007) 597–604.

[113] P. Malavita, R.M. Nerem, Fluid-induced shear stress stimulates chondrocyte proliferation partially mediated via TGF-beta1, *Tissue Eng.* 8 (2002) 581–590.

[114] M. Duan, Q. Wang, Y. Liu, J. Xie, The role of TGF- β 2 in cartilage development and diseases, *Bone Joint Res.* 10 (2021) 474–487.

[115] R. Fava, N. Olsen, J. Keski-Oja, H. Moses, T. Pincus, Active and latent forms of transforming growth factor beta activity in synovial effusions, *J. Exp. Med.* 169 (1989) 291–296.

[116] N. Johansson, U. Saarialho-Kere, K. Airola, R. Herva, L. Nissinen, J. Westermark, E. Vuorio, J. Heino, V.-M. Kähäri, Collagenase-3 (MMP-13) is expressed by hypertrophic chondrocytes, periosteal cells, and osteoblasts during human fetal bone development, *Dev. Dyn.* 208 (1997) 387–397.

[117] C. Urbach, N.C. Gordon, I. Strickland, D. Lownie, C. Joberty-Candotti, R. May, A. Herath, D. Hijnen, J.L. Thijss, C.A. Bruijnzeel-Koomen, R.R. Minter, F. Hollfelder, L. Jermutus, Combinatorial screening identifies novel promiscuous matrix metalloproteinase activities that lead to inhibition of the therapeutic target IL-13, *Chem. Bio.* 22 (2015) 1442–1452.

[118] I. Takahashi, T. Matsuzaki, H. Kuroki, M. Hoso, Disuse atrophy of articular cartilage induced by unloading condition accelerates histological progression of osteoarthritis in a post-traumatic rat model, *Cartilage* 13 (2021) 1522S–1529S.

[119] Y. Fujii, L. Liu, L. Yagasaki, M. Inotsume, T. Chiba, H. Asahara, Cartilage homeostasis and osteoarthritis, *Int. J. Mol. Sci.* 23 (2022) 6316.

[120] T. Hayami, M. Pickarski, Y. Zhuo, G. Wesolowski, G. Rodan, L. Duong, Characterization of articular cartilage and subchondral bone changes in the rat anterior cruciate ligament transection and meniscectomized models of osteoarthritis, *Bone* 38 (2006) 234–243.

[121] T. Tominari, R. Ichimaru, K. Taniguchi, A. Yumoto, M. Shirakawa, C. Matsumoto, K. Watanabe, M. Hirata, Y. Itoh, D. Shiba, C. Miyaura, M. Inada, Hypergravity and microgravity exhibited reversal effects on the bone and muscle mass in mice, *Sci. Rep.* 9 (2019) 6614.

[122] L. Gabel, A.-M. Liphardt, P.A. Hulme, M. Heer, S.R. Zwart, J.D. Sibonga, S.M. Smith, S.K. Boyd, Incomplete recovery of bone strength and trabecular microarchitecture at the distal tibia 1 year after return from long duration spaceflight, *Sci. Rep.* 12 (2022) 9446.

[123] P.J.T. Koshy, C.J. Lundy, A.D. Rowan, S. Porter, D.R. Edwards, A. Hogan, I.M. Clark, T.E. Cawston, The modulation of matrix metalloproteinase and ADAM gene expression in human chondrocytes by interleukin-1 and oncostatin M: atime-course study using real-time quantitative reverse transcription-polymerase chain reaction, *Arthritis Rheum.* 46 (2002) 961–967.

[124] M.A. Pratta, P.A. Scherle, G. Yang, R.-Q. Liu, R.C. Newton, Induction of aggrecanase 1 (ADAM-TS4) by interleukin-1 occurs through activation of constitutively produced protein, *Arthritis Rheum.* 48 (2003) 119–133.

[125] A.J. Fosang, F.M. Rogerson, C.J. East, H. Stanton, ADAMTS-5: the story so far, *Eur. Cell Mater.* 15 (2008) 11–26.

[126] N. Moulharat, C. Lesur, M. Thomas, G. Rolland-Valognes, P. Pastourea, P. Anract, F. De Ceuninck, M. Sabatini, Effects of transforming growth factor- β on aggrecanase production and proteoglycan degradation by human chondrocytes in vitro, *Osteoarthritis Cartilage* 12 (2004) 296–305.

[127] G. Zhen, Q. Guo, Y. Li, C. Wu, S. Zhu, R. Wang, X.E. Guo, B.C. Kim, J. Huang, Y. Hu, Y. Dan, M. Wan, T. Ha, S. An, X. Cao, Mechanical stress determines the configuration of TGF β activation in articular cartilage, *Nat. Commun.* 12 (2021) 1–16.

[128] M. Segarra-Queralt, M. Neidlin, L. Tio, J. Monfort, J.C. Monllau, M. González Ballester, L.G. Alexopoulos, G. Piella, J. Noailly, Regulatory network-based model to simulate the biochemical regulation of chondrocytes in healthy and osteoarthritic environments, *Sci. Rep.* 12 (2022) 1–16.

[129] P. Kahle, J.G. Saal, K. Schaudt, J. Zacher, P. Fritz, G. Pawelec, Determination of cytokines in synovial fluids: correlation with diagnosis and histomorphological characteristics of synovial tissue, *Ann. Rheum. Dis.* 51 (1992) 731–734.

[130] A.L. McNulty, N.E. Rothfusz, H.A. Leddy, P. Guilak, Synovial fluid concentrations and relative potency of interleukin-1 alpha and beta in cartilage and meniscus degradation, *J. Orthop. Res.* 31 (2013) 1039–1045.

[131] S.J. Hopkins, M. Humphreys, M.I. Jayson, Cytokines in synovial fluid. I. The presence of biologically active and immunoreactive IL-1, *Clin. Exp. Immunol.* 72 (1988) 422–427.

[132] T. Morales, M. Joyce, M. Sobel, D. Danielpour, A. Roberts, Transforming growth factor- β in calf articular cartilage organ cultures: synthesis and distribution, *Arch. Biochem. Biophys.* 288 (1991) 397–405.

[133] P.M. van der Kraan, Differential role of transforming growth factor-beta in an osteoarthritic or a healthy joint, *J. Bone Metab.* 25 (2018) 65.

[134] D.J. Leong, X.L. Gu, Y. Li, J.Y. Lee, D.M. Laudier, R.J. Majeska, M.B. Schaffler, L. Cardoso, H.B. Sun, Matrix metalloproteinase-3 in articular cartilage is upregulated by joint immobilization and suppressed by passive joint motion, *Matrix Biol.* 29 (2010) 420–426.

[135] J.D. Laubrie, S.J. Mousavi, S. Avril, About prestretch in homogenized constrained mixture models simulating growth and remodeling in patient-specific aortic geometries, *Biomech. Model. Mechanobiol.* 21 (2022) 455–469.

[136] P.G. Bush, A.C. Hall, The volume and morphology of chondrocytes within non-degenerate and degenerate human articular cartilage, *Osteoarthritis Cartilage* 11 (2003) 242–251.

[137] T. Fang, X. Zhou, M. Jin, J. Nie, X. Li, Molecular mechanisms of mechanical load-induced osteoarthritis, *Int. Orthop.* 45 (2021) 1125–1136.

[138] N. Parameswaran, S. Patial, Tumor necrosis factor- α signaling in macrophages, *Crit. Rev. Eukaryot. Gene Expr.* 20 (2010) 87–103.

[139] L.-A. Guns, S. Monteagudo, M. Kvasnytsia, G. Kerckhofs, J. Vandooren, G. Opendenakker, R.J. Lories, F. Cailotto, Suramin increases cartilage proteoglycan accumulation in vitro and protects against joint damage triggered by papain injection in mouse knees in vivo, *RMD Open* 3 (2017) e000604.